nature portfolio

Peer Review File

Nano-confinement Engineering Boosts C–N Coupling for Urea Electrosynthesis

Corresponding Author: Professor Xuanhao Wu

Attachments originally included by the reviewers as part of their assessment can be found at the end of this file.

Version 0:

Reviewer comments:

Reviewer #1

(Remarks to the Author)
This manuscript presents a comprehensive study on nano-confinement engineering of CuRu bimetallic catalysts for urea electrosynthesis via C-N coupling between CO_2 and nitrate. The work demonstrates a significant advance in urea yield (12.51 g h^{-1} $gcat^{-1}$ at 250 mA cm^{-2}) and stability (125 hours), outperforming previous benchmarks. The integration of in situ spectroscopy, computational modeling, and pore-size engineering provides mechanistic insights into how nano-confinement alters reaction pathways and intermediate retention. The study is well-structured, and the conclusions are largely supported by experimental and theoretical evidence. Overall, I recommend its publication after minor revisions. Some specific comments are provided as follows.
1. For DFT calculations, the reaction energy, zero-point energy, and entropy corrections of each intermediate in the free energy calculations should be provided in detail (listed in tables of supporting information).
2. The assignment of *OCO-*NO intermediates (Fig. 4b) needs validation. It is suggested to include reference spectra or isotopic labeling (e.g., $^{13}CO2$) to confirm peak assignments.
3. More recently reported literatures related to urea electrosynthesis can be properly cited to make this paper state-of-the-art: Adv. Mater., 2024, 36, 2402160. Adv. Energy. Mater. 2024, 14, 2401765. ACS Energy Lett., 2024, 9, 4624-4632 (highly relevant).
4. The structural information of nano-confined CuRu after durability test can be provided, if possible.
5. The volcano-shaped relationship between pore size and urea yield (Fig. 5g–h) conflicts with the monotonic increase in NO_3^- conversion (Fig. S25). Why CuRu/MCHS-11 shows higher NO_3^- conversion but lower urea selectivity than CuRu/MCHS-7

Reviewer #2

(Remarks to the Author)
The manuscript by Du et al. presents an innovative strategy to enhance the microenvironment for the electrochemical co-reduction of nitrate and carbon dioxide into urea by employing nano-confined CuRu catalysts embedded within mesoporous carbon hollow spheres (MCHS). The approach of spatially confining reactants and intermediates within nanoscale architectures is compelling and, as demonstrated, successfully increases urea production. While the study presents a strong foundation with a comprehensive set of experiments, there are several critical points that require clarification or further investigation.

1. In line 92, the authors state that CuRu nanoparticles with an average diameter of 9.16 nm were formed. However, it remains unclear whether each particle, whether located on carbon spheres (CS) or encapsulated in MCHS, contains both Cu and Ru. In Fig. S5, the authors selectively analyze individual nanoparticles to assign interplanar spacings to either Cu or Ru, but the analysis involves different particles. Moreover, in line 134, they acknowledge the difficulty of alloying Cu and Ru, which raises further doubts. Given the extensive characterization presented, the authors should clearly articulate their interpretation regarding the existence—or absence—of a bimetallic phase.

2. In line 123, the statement that the valence state of Cu is “between +0 and +1” would benefit from refinement. A more accurate phrasing would acknowledge the presence of both metallic Cu and Cu(I) oxide phases.

3. In line 141 and Fig. S8, the authors discuss differences in double-layer capacitance among catalysts, reflecting variations in electrochemically active surface area (ECSA). However, in line 501, they mention that current densities were normalized by geometric area. This discrepancy could lead to misleading comparisons across catalysts. The authors should clarify whether current densities are normalized by geometric or ECSA and use consistent notation throughout the manuscript.

4. In line 162 (caption of Fig. 3), the authors note that no iR compensation was applied. Since the different catalysts may have varying conductivities, not accounting for ohmic drop could affect the accuracy of potential comparisons.

5. Although the identification of urea using NMR is valid, the quantification based solely on a urease-based assay could be problematic. This method has been shown to overestimate urea concentrations, particularly in the presence of high ammonium levels (https://doi.org/10.1016/j.cej.2022.139836). Additional quantification techniques or validation would strengthen the conclusions.

6. Electrolysis tests for individual CO2 and nitrate reduction are essential to isolate and understand side product formation during co-reduction. Currently, faradaic efficiency (FE) values are incomplete—up to 20% unaccounted for in MCHS (Fig. 3b) and up to 40% in CS (Fig. S15). These gaps highlight the need for further product analysis.

7. The reasoning behind electrolyte selection should be better explained. For instance, why is potassium bicarbonate used only in the absence of nitrate? As bicarbonate can buffer CO2 availability, this discrepancy could affect the comparability of results under different reaction conditions.

8. The authors should specify the Cu:Ru ratios used in Figs. 3a and 3b and explain the omission of the 24:1 ratio from Fig. 3c.

9. From Fig. 3, it is evident that ammonium is the dominant product in terms of FE. However, in lines 213–215, the ATR-SEIRAS spectra are interpreted to suggest that hydrogenation to form *NH2 is suppressed during CO2–$NO3^-$ co-reduction. This interpretation appears contradictory, given the high ammonium production observed. The authors should reconcile these findings.

10. Reporting the initial and final pH values for electrolysis experiments is important. Changes in pH due to reduction reactions can influence both the reaction environment and the calibration of the applied potential vs. RHE.

11. In lines 281–285, the authors suggest that a pore size of 7 nm optimizes urea synthesis, but the mechanistic basis for this observation is not discussed. Possible explanations (e.g., optimal confinement effects, mass transport considerations, or surface accessibility) should be explored.

12. In Fig. 6a, the authors show a significant decrease in urea yield when switching from H2O to D2O, indicating that C–N coupling may involve *H. The authors briefly suggest this in line 615, but the mechanistic implications deserve further elaboration.

Overall, this study proposes a promising strategy for improving urea production via the co-reduction of CO2 and nitrate, and the integration of nanoconfinement principles with bifunctional metal catalysts is noteworthy. However, the manuscript would benefit significantly from clearer interpretation of characterization data, consistent reporting of electrochemical metrics, and a more detailed mechanistic discussion. Addressing these concerns—either through improved explanation or additional experimentation—will strengthen the scientific rigor and impact of the work.

Reviewer #3

(Remarks to the Author)
The manuscript entitling “Nano-confinement Engineering Boosts C–N Coupling for Urea Electrosynthesis” presents an in-depth study on the electrosynthesis of urea via the co-reduction of CO_2 and nitrate using a nano-confined CuRu bimetallic catalyst within mesoporous carbon hollow spheres (MCHS). The authors demonstrate how nano-confinement architecture significantly improves urea yield, selectivity, and reaction kinetics by altering intermediate species and enhancing transport properties. The work combines comprehensive experimental characterization with in situ spectroscopies and DFT simulations to elucidate the mechanism, presenting an excellent and timely research. With minor clarification on mechanisms, catalyst optimization, and reproducibility details, the manuscript will be suitable for publication in a high-impact journal like Nature Communications.
1. While the switching from *COOH–$*NH_2$ to *OCO–*NO is discussed, a clearer visual or tabulated comparison of energy barriers and reaction paths between confined and non-confined catalysts would enhance readability. The authors are requested to go through the following manuscript: doi.org/10.1021/acs.jpclett.1c03242.
2. The Ru loading is extremely low (Cu:Ru = 24:1). The rationale behind this choice and its optimization deserves further discussion.
3. The urea FE remains moderate (~16.5%). While high current density is achieved, discussion on improving selectivity further would add depth. Please see doi.org/10.1002/adfm.202200882 and other relevant papers.
4. Table S7 compares performance with other catalysts. It would be more effective to bring a brief version into the main text for quick reader access.

Reviewer #4

(Remarks to the Author)
In this manuscript, the authors developed a catalyst of CuRu bimetallic on mesoporous carbon hollow spheres (CuRu/MCHS) for urea synthesis. The authors have designed this catalyst material and conducted comprehensive experimental characterization, demonstrating the uniform dispersion of CuRu nanoparticles within the carbon layer and systematically investigating the metal valence states. However, the catalytic performance shows a considerable gap compared with most reported materials in the literature. Furthermore, several critical factors were overlooked in the DFT calculations, leading to insufficiently clear interpretation of the reaction mechanism. Therefore, based on the identified limitations in both catalytic performance and theoretical analysis, I conclude that this manuscript does not meet the scientific standards required for publication in Nature Communications. My main concerns are as follows:
1. The figure citation in the manuscript contains an error: "Fig. 2i-2k" should be corrected to "Fig. 1i-1k".
2. The peak positions labeled for CuRu/MCHS and Ru/MCHS in Fig. 2c are incorrect.
3. The XANES analysis demonstrates that the Cu species in both CuRu/MCHS and Cu/MCHS catalysts exhibit mixed valence states between Cu(0) and Cu(I), as evidenced by the characteristic Cu-O bonding in Fig. 1f, indicating partial oxidation of Cu. However, the origin of this oxidation state (whether intrinsic to the synthesis process or resulting from post-synthetic air exposure) remains unaddressed, and the relative proportions of Cu(0) and Cu(I) species have not been quantitatively determined.
4. The reported catalyst exhibits a maximum urea Faradaic efficiency of merely 16.5%, significantly lower than the benchmark performance (>30%) achieved by most state-of-the-art catalysts in literature. Such inferior catalytic activity would severely limit its practical application for efficient urea synthesis.
5. The Faradaic efficiency for urea production was not evaluated in the flow cell system, which represents a critical electrochemical metric for evaluating catalytic performance
6. The presented DFT calculations are notably incomplete as the authors neither consider the essential control cases of urea synthesis on pure Cu and pure Ru for mechanistic comparison, nor do they consider the potential role of the MCHS support structure.

Version 1:

Reviewer comments:

Reviewer #1

(Remarks to the Author)
The authors have positively responded all the comments raised by the reviewers. Therefore, I recommend the acceptance of this paper for publication.

Reviewer #2

(Remarks to the Author)
The authors have thoroughly and thoughtfully addressed all the comments and concerns raised in the initial review. The revised manuscript now presents a much clearer and more convincing discussion of the results, with improved data interpretation and consistency throughout. I recommend the manuscript for publication in its current form.

Reviewer #3

(Remarks to the Author)
The authors have carefully addressed all the concerns raised in the previous version of the manuscript. I now recommend its publication as is.

Reviewer #4

(Remarks to the Author)
In the revised manuscript, the authors have addressed the concerns suggested by the reviewers with additional experiment data and detailed discussions, which is quite helpful to further improve the quality of the manuscript. The reviewer thus suggests the acceptance of the revised version of this work.

Response to Reviewers' Comments

Article Title: Nano-confinement Engineering Boosts C–N Coupling for Urea Electrosynthesis

Manuscript ID: NCOMMS-25-37260

Dear Reviewers,

Thank you for your helpful comments and suggestions on modifying our manuscript and giving us the opportunity to make those changes. After careful consideration, we have revised the manuscript accordingly, and the detailed corrections are listed below point by point. We also highlighted our revisions in the manuscript in red so that you could easily identify them. We hope that these revisions and responses will be satisfactory. Thank you again for your time and support.

Blue-colored texts indicate our response to reviewers' comments.

Red-colored texts indicate changes made in the revised manuscript.

Reviewer 1

Comments: *This manuscript presents a comprehensive study on nano-confinement engineering of CuRu bimetallic catalysts for urea electrosynthesis via C-N coupling between CO_2 and nitrate. The work demonstrates a significant advance in urea yield (12.51 g h^{-1} $gcat^{-1}$ at 250 mA cm^{-2}) and stability (125 hours), outperforming previous benchmarks. The integration of in situ spectroscopy, computational modeling, and pore-size engineering provides mechanistic insights into how nano-confinement alters reaction pathways and intermediate retention. The study is well-structured, and the conclusions are largely supported by experimental and theoretical evidence. Overall, I recommend its publication after minor revisions. Some specific comments are provided as follows.*

Response: We sincerely value your thoughtful recognition and deeply appreciate the supportive comments on our work. We have carefully addressed your concerns in the revised manuscript, providing additional clarifications, data, and discussions where needed. Below, we detail our point-by-point responses to your specific comments. Thank you again for your time and effort.

1. For DFT calculations, the reaction energy, zero-point energy, and entropy corrections of each intermediate in the free energy calculations should be provided in detail (listed in tables of supporting information).

Response: Thank you for this constructive suggestion. We have now provided detailed data for the reaction energy, zero-point energy, and entropy corrections for all calculated intermediates involved in the free energy calculations. In the revised manuscript, following the suggestion of Reviewer 4 (Comment 6), we have recalculated the DFT to include consideration of the potential role of the MCHS support structure. These values and the calculation methods are now included in **Tables S10** and **Table S12** in the Supporting Information. We appreciate your suggestion which helps improve the transparency and reproducibility of our DFT results.

The relevant revisions are presented as follows:

Supplementary information txt: "The computational hydrogen electrode (CHE) model was adopted to calculate the Gibbs free energy change (ΔG) for each elementary step as follows:

$$\Delta G = \Delta E + \Delta E_{ZPE} - T\Delta S \quad (S2)$$

where ΔE represents the electronic energy contribution directly derived from DFT calculations. ΔE_{ZPE} and $T\Delta S$ denote the contributions of zero–point energy and entropy (at 298.15 K), respectively. The vibrational frequency for intermediates can be computed accordingly (**Table S10** and **Table S12**)."

Supplementary Table S10| The calculated ΔE, ΔE_{ZPE} and $T\Delta S$ of various species along the reaction pathways for urea synthesis on the CuRu model .

Species	ΔE (eV)	ΔE_{ZPE} (eV)	$T\Delta S$ (eV)
HNO_3	-28.59	0.71	0.35
$*CO_2$	-1111.39	0.28	0.35
*COOH	-1115.20	0.60	0.38
$*CO_2NO$	-1126.15	0.53	0.45
$*CO_2NHO$	-1131.06	0.88	0.46
$*CO_2NHOH$	-1134.75	1.19	0.51
$*CO_2NH$	-1125.32	0.76	0.34
$*CO_2NH_2$	-1129.45	1.11	0.41
$*COOHNH_2$	-1132.78	1.39	0.51
$*CONH_2$	-1120.86	0.94	0.36
$*ONCONH_2$	-1135.95	1.23	0.41
$*CO(NH_2)$	-1137.96	1.77	0.44
$*CO_2$+*NO	-1126.71	0.50	0.65
$*CO_2$+*NHO	-1131.21	0.79	0.70
$*CO_2$+*NHOH	-1135.58	1.09	0.71
$*CO_2$+*NH	-1125.76	0.66	0.49
$*CO_2$+$*NH_2$	-1130.19	0.98	0.52
*COOH+$*NH_2$	-1133.12	1.27	0.68

Supplementary Table S12| The calculated ΔE, ΔE_{ZPE} and $T\Delta S$ of various species along the reaction pathways for urea synthesis on the Cu model .

Species	ΔE (eV)	ΔE_{ZPE} (eV)	$T\Delta S$ (eV)
$*CO_2$	-1088.34	0.28	0.35
*COOH	-1091.85	0.60	0.38
$*CO_2NO$	-1101.90	0.50	0.49
$*CO_2NHO$	-1106.45	0.84	0.51
$*CO_2NHOH$	-1110.58	1.16	0.66
$*CO_2NH$	-1101.16	0.76	0.40
$*CO_2NH_2$	-1105.58	1.08	0.53
$*COOHNH_2$	-1108.72	1.38	0.57

*2. The assignment of *OCO-*NO intermediates (Fig. 4b) needs validation. It is suggested to include reference spectra or isotopic labeling (e.g., $^{13}CO_2$) to confirm peak assignments.*

Response: Thank you for your insightful comment and attention to experimental details. We believe your suggestion has been very helpful in improving our understanding of the reaction mechanism. Based on your recommendation, we carefully re-examined all the infrared spectra as well as the relevant literature regarding peak assignments. The corresponding reference spectra have been compiled and included in the Response Letter for reference.

1. Spectral interpretation of *OCO and *COOH intermediates

Due to experimental limitations, we were unable to obtain $^{13}CO_2$, and thus isotope labeling experiments could not be performed. In order to better distinguish between *OCO and *COOH species in the absence of isotope-labeling experiments, we have reviewed and cited literature that presents infrared spectra showing both characteristic peaks concurrently.

a. As shown in **Table R1**, the study by Shao et al. confirmed that on a Cu surface in 0.1 M $KHCO_3$, the peak at 1400 cm^{-1} is attributed to the COO^- species, while the peak at 1370 cm^{-1} corresponds to the *COOH intermediate. The original description is as follows: "*Two other weak bands observed near 1380 (*COOH) and 1400 (bidentate COO^-) cm^{-1} from −0.4 to −0.9 V implied the coexistence of these two intermediates after the initial electron transfer and protonation on CO_2 molecules.*" (*J. Am. Chem. Soc.* 139, 15664–15667 (2017))

b. This observation is further supported by the work of Smith et al., where, as shown in **Fig. R1**, both the predicted positions and experimental detection of characteristic peaks corresponding to various intermediates were reported under ATR-FTIR analysis. (*ACS Catal.* 7, 1, 606–612 (2017))

c. Liu et al., in their study on Ti-MOF-based electrocatalysts for urea synthesis, attributed an upward peak at ≈1408 cm^{-1} to the *OCO species, noting its presence in both co-reduction and CO_2RR. The original description is as follows: "*The upward peak ≈1408 cm^{-1} was ascribed to*

**OCO species, and this signal is present in both co-reduction and CO_2RR.*" (*Adv. Funct. Mater.* 34, 2400892 (2014))

In our ATR-SEIRAS spectra, as shown in **Fig. 4c**, the CuRu/MCHS sample exhibits a distinct characteristic peak at 1395 cm^{-1}, while no observable peak appears at 1408 cm^{-1}. In contrast, as shown in **Fig. 4e**, the CuRu/CS sample displays a clear peak at 1408 cm^{-1}, with only a very weak signal at 1395 cm^{-1}. Based on the conclusions of the aforementioned studies, we reasonably attribute the peak at 1408 cm^{-1} to the *OCO species (bidentate COO^-), and the peak at 1395 cm^{-1} to the *COOH intermediate.

Table R1| Summary of detected intermediates and corresponding band positions in CO_2RR

Surface	Electrolyte	Band center (cm^{-1})	Assignment
Cu	CO_2-sat. 0.1 M $KHCO_3$	1400	COO^-, two O coordinated
		1380	COOH, C coordinated

Reference: *J. Am. Chem. Soc.* 139, 15664–1566 (2017)

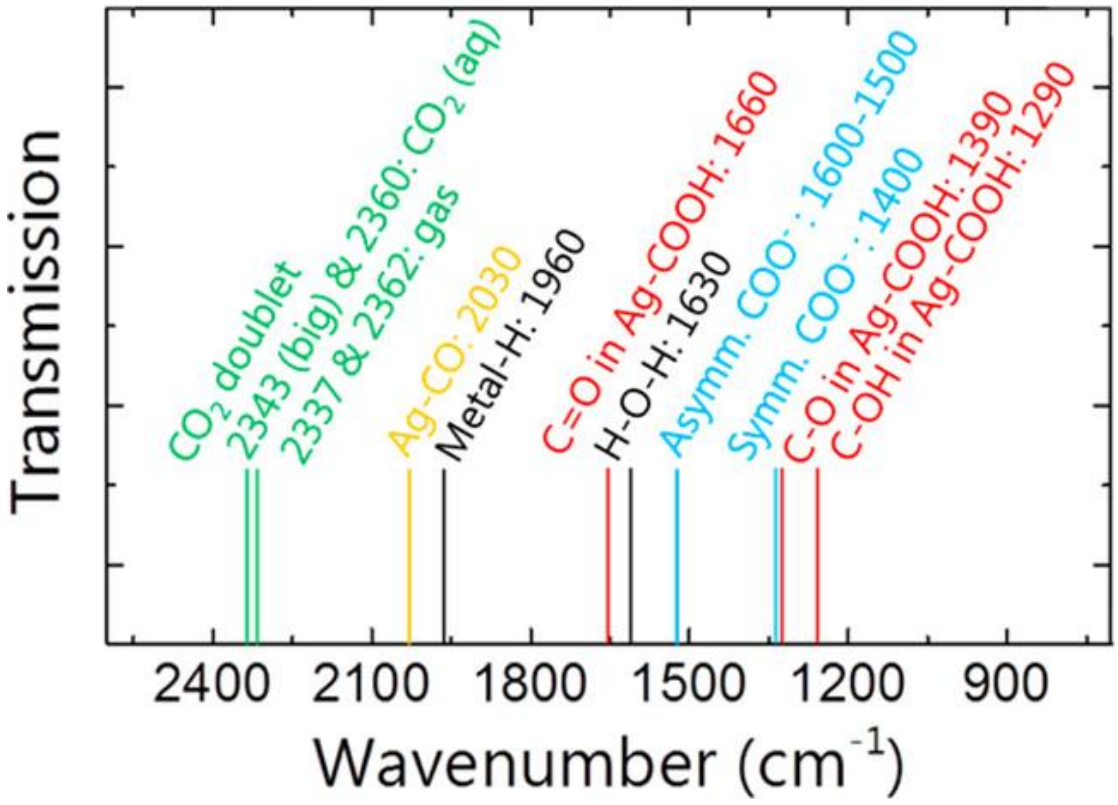

Fig. R1. Predicted locations for the different reactants, products, and intermediates that are present during the ATR-FTIR experiments. The CO_2 doublet is shown in green, CO is shown

in yellow, the COOH intermediate signals are shown in red, the COO^- intermediate signals are shown in blue, and black represents water and hydrogen. (*ACS Catal.* 7, 1, 606–612(2017))

2. Spectral interpretation of *NO intermediates

As shown in **Fig. R2**, Chu et al. attributed the characteristic peak around ~1880 cm^{-1} in the in situ FTIR spectra of electrocatalytic NO reduction to adsorbed NO. (*ACS Catal. 13, 14*, 9550–9557 (2013)) Similarly, in a study on urea synthesis via co-reduction of CO_2 and NO_3^-, Wang et al. assigned the peak at 1888 cm^{-1} to the *NO intermediate species. (*J. Am. Chem. Soc.* 144, 26, 11530–11535 (2022))

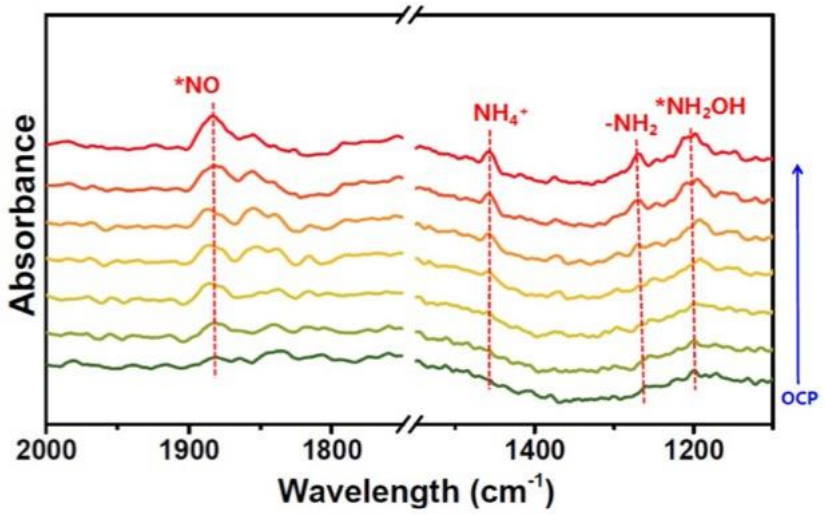

Fig. R2. In situ FTIR spectra of W_1Pd from OCP to −0.4 V. (*ACS Catal.* 13, 14, 9550–9557 (2023))

Based on the above considerations, we have supplemented the revised manuscript with reference spectra to support the peak assignments. The corresponding peak positions and reference spectra for the relevant intermediates are now included in **Tables S9** in the Supporting Information.

The relevant revisions are presented as follows:

Line 246: "The characteristic peaks at 1890 cm^{-1} and 1408 cm^{-1} were assigned to *NO[48,49] and *OCO[50-53] species (**Table S9**), demonstrating their important correlation with urea generation."

Supplementary Table S9| The assignment of intermediates.

Assignment	Band center (cm^{-1})	Reference
*OCO	~1408	Adv. Funct. Mater. 2024, 34, 2400892 ACS Energy Lett. 2019, 4, 3, 682–689 J. Am. Chem. Soc. 2017, 139, 44, 15664–15667 ACS Catal. 2017, 7, 1, 606–612
*COOH	~1395	ACS Catal. 2017, 7, 606-612 Adv. Funct. Mater. 2021, 2104243 Angew. Chem. Int. Ed. 2022, 61, e20211391842
*CO	~2050	ACS Nano 2022, 16, 9095-9104 ACS Catal. 2020, 10, 15, 8049–8057
*NO	~1890	J. Am. Chem. Soc. 2022, 144, 11530-11535 ACS Catal. 2023, 13, 14, 9550–9557 Inorg. Chem. 2024, 63, 45, 21387–21396
*NH_2	~1177-1170	Angew. Chem. Int. Ed. 2024, 63, e202402215 Angew. Chem. Int. Ed. 2025, 64, e202414392 Nat. Sustain. 2021, 4, 868–876
*NH_2	~3345-3350	Angew. Chem. Int. Ed. 2025, 64, e202413534
C-N	~1425	Nat. Commun. 2024, 15, 176
N-C-N	~1477	Nat. Commun. 2024, 15, 176

Newly added references:

48 Chen, K. *et al.*. Atomically dispersed W_1–O_3 bonded on Pd metallene for cascade NO electroreduction to NH_3. *ACS Catal.* **13**, 9550-9557 (2023).

49 Wei, X. *et al.* Oxygen vacancy-mediated selective C–N coupling toward electrocatalytic urea synthesis. *J. Am. Chem. Soc.* **144**, 11530-11535 (2022).

50 Zhu, S. *et al.* Direct observation on reaction intermediates and the role of bicarbonate anions in CO_2 electrochemical reduction reaction on Cu surfaces. *J. Am. Chem. Soc.* **139**, 15664-15667 (2017).

51 Liu, X. *et al.* High C-selectivity for urea synthesis through O-philic adsorption to form *OCO intermediate on Ti-MOF based electrocatalysts. *Adv. Funct. Mater.* **34**, 2400892 (2024).

52 Firet, N. J. & Smith, W. A. Probing the reaction mechanism of CO_2 electroreduction over Ag films via operando infrared spectroscopy. *ACS Catal.* **7**, 606-612 (2017).

53 Zhu, S. *et al.* CO_2 electrochemical reduction as probed through infrared spectroscopy. *ACS Energy Lett.* **4**, 682-689 (2019).

3. More recently reported literatures related to urea electrosynthesis can be properly cited to make this paper state-of-the-art: Adv. Mater., 2024, 36, 2402160. Adv. Energy. Mater. 2024, 14, 2401765. ACS Energy Lett., 2024, 9, 4624-4632 (highly relevant).

Response: We sincerely thank you for highlighting these important and timely contributions. In fact, the two studies mentioned ($CuPd_1Rh_1$-DAA and Cu_1Ru) were previously considered in the comparative analysis of our original manuscript in **Table S8**, although not explicitly cited in the main text. In the revised manuscript, we have now appropriately cited all three references, acknowledging their relevance to the development of Cu-based electrocatalysts for urea synthesis. These additions further enhance the context and demonstrate the significance of our nano-confinement strategy within the state-of-the-art research landscape.

The relevant revisions are presented as follows:

Line 42: "Designing multimetallic catalysts with distinct catalytic sites have been proposed as effective strategies for C–N coupling[8-15]."

Newly added references:

13 Wang, F. *et al.* Selective urea electrosynthesis from nitrate and CO_2 on isolated copper alloyed ruthenium. *ACS Energy Lett.* **9**, 4624-4632 (2024).

14 Du, W. *et al.* Synergistic Cu single atoms and MoS_2-edges for tandem electrocatalytic reduction of NO_3^- and CO_2 to urea. *Adv. Energy Mater.* **14**, 2401765 (2024).

15 Chen, K. *et al.* Urea electrosynthesis from nitrate and CO_2 on diatomic alloys. *Adv. Mater.* **36**, 2402160 (2024).

4. The structural information of nano-confined CuRu after durability test can be provided, if possible.

Response: We sincerely thank you for this valuable suggestion. We agree that providing detailed structural information of the catalyst after the durability test is crucial for evaluating its long-term stability. In response, we have now supplemented the revised manuscript with additional HAADF-STEM characterization of the post-reaction catalyst, enabling precise measurement of the metal particle size and offering deeper insight into its structural evolution (**Fig. S20**). Furthermore, the previously included XPS data confirm that the metal valence states remained largely unchanged, while HRTEM imaging verifies that the carbon framework of CuRu/MCHS was well preserved without structural collapse. These comprehensive post-reaction analyses collectively reinforce the outstanding structural robustness of our nano-confined catalyst.

The relevant revisions are presented as follows:

Line 216: "The chemical valence states of Cu and Ru remained largely unchanged after the reaction (**Fig. S19**). The CuRu nanoclusters maintained a uniform dispersion with an average diameter of 2.39 ± 1.21 nm and showed no obvious aggregation. Moreover, the hollow cavity structure and mesoporous channels were well preserved (**Fig. S20**)."

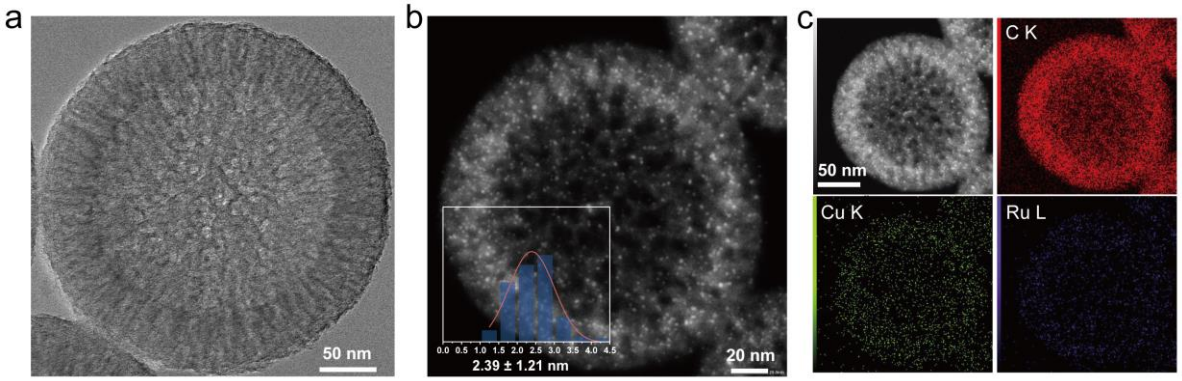

Supplementary Fig. S20| Structural information of CuRu/MCHS after electrocatalysis. a, HR-TEM image of CuRu/MCHS after electrocatalysis. **b**, HAADF-STEM characterization and particle size distribution of CuRu/MCHS after stability test. **c**, EDS mapping profile of CuRu/MCHS after stability test.

5. The volcano-shaped relationship between pore size and urea yield (Fig. 5g–h) conflicts with the monotonic increase in NO_3^- conversion (Fig. S25). Why CuRu/MCHS-11 shows higher NO_3^- conversion but lower urea selectivity than CuRu/MCHS-7.

Response: We sincerely thank you for raising this insightful question regarding the relationship between pore size, NO_3^- conversion, and urea selectivity. We agree that the observed trend, where NO_3^- conversion increases monotonically with pore size while urea selectivity exhibits a volcano-shaped dependence, is a key point that merits clarification.

Our experimental data indicate that although CuRu/MCHS-11 achieves the highest nitrate conversion (38.6%), its urea-N selectivity (9.5%) is significantly lower than that of CuRu/MCHS-7 (19.0%). This suggests that higher NO_3^- conversion does not necessarily lead

to higher urea yield, as the reaction pathway is strongly influenced by the nano-confinement environment.

We attribute this behavior to the dual role of pore size in regulating reactant transport and intermediate confinement:

1. Larger pores (e.g., 11 nm) facilitate NO_3^- diffusion into the cavity, as confirmed by FEM simulations showing a higher NO_3^- interior/exterior concentration ratio (C_I/C_E = 0.954 for 11 nm vs. 0.919 for 7 nm). This enhances NO_3^- accessibility and overall conversion. However, the weakened confinement in larger pores would also accelerate the outward diffusion of key intermediates, reducing their effective retention time and probability of C–N coupling. This is supported by the lower C_I/C_E ratio of urea in CuRu/MCHS-11 (1.34) compared to CuRu/MCHS-7 (1.62).

2. Analysis of the product distribution reveals that pore size influences the distribution of reaction products. As shown in **Fig. 5i**, CuRu/MCHS-11 exhibits a relatively higher selectivity toward NO_2^- compared to the CuRu/MCHS-7, with values of 13.2 ± 1.7% versus 10.6 ± 0.7%, respectively.

Therefore, it is reasonable to speculate that for CuRu/MCHS-11, more NO_3^- was converted into NO_2^-; however, due to its weaker confinement capability toward reaction intermediates, NO_2^- is relatively less likely to be further reduced to the key intermediate *NO and effectively retained. This hinders its subsequent coupling with carbon-containing intermediates to form urea. These findings highlight that while higher nitrate conversion allows more reactants to participate in the reaction, the selectivity toward urea is dominantly governed by intermediate confinement rather than conversion rates alone. We have added further discussion on the conversion rate and selectivity in the revised manuscript. We sincerely appreciate your constructive comments.

The relevant revisions are presented as follows:

Line 344: "Notably, NO_3^- conversion rates after 30 minutes of electrolysis at –1.1 V (vs. RHE) increased with pore size (26.9%, 35.9%, and 38.6% for 4, 7, and 11 nm, respectively), indicating that urea production was not solely governed by nitrate conversion (**Fig. S31**). In

contrast, the larger-pore CuRu/MCHS-11 favored the conversion of NO_3^- to NO_2^-, with FE(NO_2^-) ranging from 23.5% to 13.2% between –0.7 and –1.1 V (vs. RHE), compared to 16.5%–10.6% for CuRu/MCHS-7 under the same conditions (**Fig. 5i**). This suggests that the enhanced NO_3^- conversion in CuRu/MCHS-11 was not effectively directed toward urea formation, which can be attributed to the diminished nanoconfinement effect impairing the retention of key intermediates and thus the efficiency of C–N coupling."

Reviewer 2

Comments: *The manuscript by Du et al. presents an innovative strategy to enhance the microenvironment for the electrochemical co-reduction of nitrate and carbon dioxide into urea by employing nano-confined CuRu catalysts embedded within mesoporous carbon hollow spheres (MCHS). The approach of spatially confining reactants and intermediates within nanoscale architectures is compelling and, as demonstrated, successfully increases urea production. While the study presents a strong foundation with a comprehensive set of experiments, there are several critical points that require clarification or further investigation.*

Response: We sincerely appreciate your recognition of our work. We are pleased that the strategy of nano-confinement to enhance urea production was found compelling. Your thorough consideration and guidance have greatly enhanced the rigor and depth of this work. We have carefully addressed all the critical points raised in the revised manuscript, providing additional clarifications, experimental data, and discussion where necessary. Below, we detail our point-by-point responses to your specific comments. Once again, thank you for your time and effort, which has significantly strengthened this work.

1. In line 92, the authors state that CuRu nanoparticles with an average diameter of 9.16 nm were formed. However, it remains unclear whether each particle, whether located on carbon spheres (CS) or encapsulated in MCHS, contains both Cu and Ru. In Fig. S5, the authors selectively analyze individual nanoparticles to assign interplanar spacings to either Cu or Ru, but the analysis involves different particles. Moreover, in line 134, they acknowledge the difficulty of alloying Cu and Ru, which raises further doubts. Given the extensive characterization presented, the authors should clearly articulate their interpretation regarding the existence—or absence—of a bimetallic phase.

Response: We thank you for raising this important point regarding the precise configuration of Cu and Ru in our catalysts. We agree that clarifying the nature of the bimetallic phase is essential.

As correctly noted, the HRTEM images in **Fig. S5**, which show lattice fringes corresponding to Cu or Ru, were acquired from different particles. This was due to practical limitations in resolving distinct metallic domains within individual nanoparticles under beam-sensitive

conditions. To gain more definitive insight into the elemental distribution, we performed additional EDS mapping and aberration-corrected HAADF-STEM on individual nanoparticles.

These analyses revealed a spatial overlap of Cu and Ru signals within the same nanoparticles in both CuRu/CS and CuRu/MCHS. In CuRu/CS, Cu was uniformly dispersed on the carbon support, while Ru appeared in a looser distribution over the Cu-rich regions. For CuRu/MCHS, AC HAADF-STEM observations were conducted over multiple regions. The measured lattice fringes confirmed the coexistence of Cu and Ru in adjacent and partially overlapping spatial domains. The measured interplanar spacings did not correspond to those characteristic of a CuRu alloy structure.

We attempted to perform EDS mapping in AC-HAADF-STEM on the small nanoparticles in CuRu/MCHS to further confirm the distribution of Cu and Ru within the overlapping regions. Unfortunately, we found that nanoparticles of 1–2 nm exhibited migration and re-dispersion during the EDS mapping measurement. This beam-induced migration is primarily attributed to the high surface energy and structural instability of such ultrasmall metallic nanoparticles. Consequently, it was challenging to accurately image individual particles; therefore, multiple images were provided to more reliably determine the lattice fringe spacings.

These observations are consistent with our EXAFS fitting results, which indicated no significant Cu-Ru coordination, thus ruling out the formation of a homogeneous alloy. Therefore, we conclude that Cu and Ru coexist primarily as adjacent or interfaced monometallic domains rather than forming alloy phases. We have included the additional data in the Supporting Information and revised the manuscript text accordingly to reflect this interpretation.

The relevant revisions are presented as follows:

Line 92: "CuRu nanoparticles (average diameters of 9.16 ± 3.69 nm) were loaded in an amorphous form on the surface of the carbon sphere, with Cu uniformly dispersed on the carbon support and Ru distributed more loosely over the Cu-rich regions (**Fig. S2**)**."**

Line 103: "The lattice stripes with spacings of Cu(111) (0.208 nm), Ru(100) (0.233 nm) and Ru(002) (0.224 nm) crystal surfaces were identified in aberration-corrected HAADF-STEM

images of single nanocluster (**Fig. S5**). No characteristic lattice spacings of the CuRu alloy were observed[33,34], indicating that Cu and Ru coexist primarily as adjacent or interfaced monometallic domains.**"**

Line 133: "In combination with the AC HAADF-STEM images, these results strongly indicate that a Cu–Ru alloyed structure was not formed, or, if present, its proportion is negligible[38,39].**"**

Supporting Information txt: "Aberration-corrected high-angle annular dark-field scanning transmission electron microscopy (AC HAADF-STEM) images were taken from JEM-ARM300F2 (JEOL).**"**

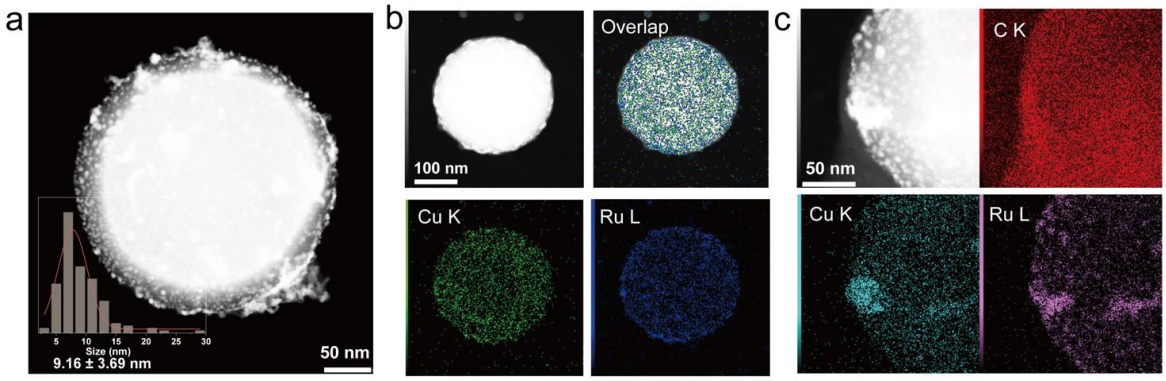

Supplementary Fig. S2| HAADF-STEM and EDS mapping of CuRu/CS. a, HAADF-STEM characterization and particle sizes distribution of CuRu/CS. **b**, EDS mapping profile of a single CuRu/CS. **c**, EDS mapping profile of localized enlarged area of CuRu/CS.

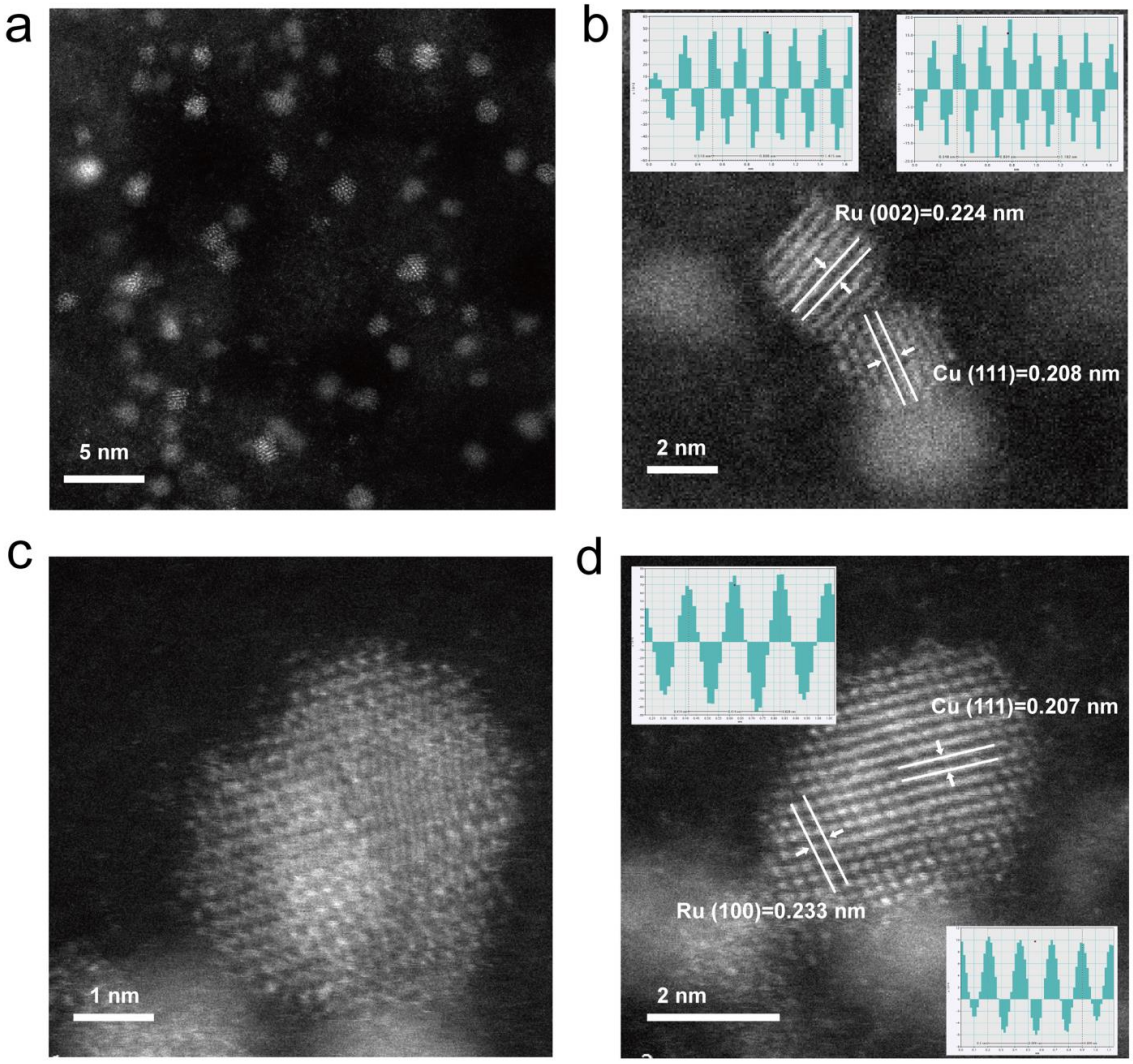

Supplementary Fig. S5| AC HAADF-STEM characterization of CuRu/MCHS. a, AC HAADF-STEM image of the cavity region of CuRu/MCHS. **b-d**, AC HAADF-STEM image of individual nanoclusters in CuRu/MCHS with calculated interplanar distances.

Newly added references:

33 Liu, Y. *et al.* Boosting the Volmer step by synergistic coupling of dilute CuRu nanoalloy with Cu/Ru dual single atoms for efficient and CO-tolerant alkaline hydrogen oxidation. *Chinese J. Catal.* **72**, 266-276 (2025).

34 Chen, S. *et al.* Engineering Cu/Ru heterointerface-shelled nanocavities by the kirkendall effect for highly efficient nitrate electroreduction to ammonia. *J. Am. Chem. Soc.* **147**, 36494-36507 (2025).

2. In line 123, the statement that the valence state of Cu is "between +0 and +1" would benefit from refinement. A more accurate phrasing would acknowledge the presence of both metallic Cu and Cu(I) oxide phases.

Response: Thank you for pointing this out. We have revised the statement accordingly to more accurately describe the valence state of Cu, clearly indicating the coexistence of Cu^0 and Cu^+ phases in the sample. The relevant content was updated in the manuscript.

The relevant revisions are presented as follows:

Line 121: "In X-ray absorption near-edge structure (XANES), the Cu K-edge spectra showed that the pre-edge absorption energy of CuRu/MCHS and CuRu/CS were located between those of Cu foil and Cu_2O references, implying the coexistence of metallic Cu (Cu^0) and Cu(I) oxide (Cu^+) phases (**Fig. 2d**)."

3. In line 141 and Fig. S8, the authors discuss differences in double-layer capacitance among catalysts, reflecting variations in electrochemically active surface area (ECSA). However, in line 501, they mention that current densities were normalized by geometric area. This discrepancy could lead to misleading comparisons across catalysts. The authors should clarify whether current densities are normalized by geometric or ECSA and use consistent notation throughout the manuscript.

Response: We thank you for this careful observation and for highlighting the need for clarity in current density normalization. In response, we have thoroughly reviewed the relevant data presentation throughout the manuscript and confirmed that all current densities are normalized by geometric area. To address the underlying concern regarding ECSA differences, we have now calculated the ECSA for each catalyst using the roughness factor derived from double-layer capacitance (C_{dl}) measurements (*Chem. Sci.* 16, 10042-10050 (2025)). The detailed calculation procedure has been added to the Materials and Methods section. This supplementary analysis provides further insight into the intrinsic activity differences among the catalysts, while ensuring consistent and unambiguous comparison based on geometric area normalization in all figures and discussions

The relevant revisions are presented as follows:

Line 145: "Electrochemical impedance spectra (EIS) and cyclic voltammetry (CV) curves showed that compared to CuRu/CS, CuRu/MCHS had lower charge transfer resistance (R_{ct}), faster ion diffusion, higher double-layer capacitance (C_{dl}) (775 μF cm^{-2} vs. 491 μF cm^{-2}) and electrochemical active surface area (ECSA) (36.9 cm^2 vs. 23.4 cm^2) (**Fig. S8**)."

Line 548: "All current densities were normalized by geometric area, and the geometric area of all tested working electrodes was 1×1 cm^2."

Line 550: "The linear slope was equivalent to twice of the double-layer capacitance C_{dl}, and the electrochemical active surface area (ECSA) of catalyst was calculated by the following equation and normalized to geometric area: ECSA = R_f×S = (C_{dl}/C_s)×S. S stands for the real surface area of the smooth metal electrode, which was generally equal to the geometric area of carbon paper electrode (in this work, S = 1.0 cm^2). The roughness factor R_f was estimated from the ratio of double-layer capacitance C_{dl}. The catalyst loading was maintained at 0.02 mg cm^{-2}. Cs was the specific capacitance under identical electrolyte conditions, 21 μF cm^{-2} was used in this work[70]."

Newly added references:

70 Yang, F. *et al.* Bismuthene for highly efficient carbon dioxide electroreduction reaction. *Nat. Commun.* **11**, 1088 (2020).

4. In line 162 (caption of Fig. 3), the authors note that no iR compensation was applied. Since the different catalysts may have varying conductivities, not accounting for ohmic drop could affect the accuracy of potential comparisons.

Response: We appreciate your insightful question. We acknowledge that differences in catalyst conductivity can indeed influence the observed potentials due to varying ohmic losses. In our experiments, no *i*R compensation was applied in order to present the raw electrochemical behavior of the catalysts. All electrochemical measurements were performed under identical conditions using the same electrode configuration and electrolyte.

We agree that differences in catalyst conductivity may lead to variations in ohmic resistance, which can affect the accuracy of potential comparisons. To verify the influence of ohmic drop, we performed *i*R compensation using resistance values obtained from EIS measurements and included the original LSV curves for comparison. (**Fig. S9** and **Fig. S29**). The *i*R -correction rate was set 85%, following established practice (*ACS Energy Lett.* 8, 4, 1952–1958 (2023)).

The results show that although the absolute potentials slightly shift after *i*R correction, the overall activity trend among the catalysts remains consistent. We provided the solution resistance (*R*s) for each catalyst and the *i*R-corrected potentials at the corresponding current densities (see **Fig. S9** and **Fig. S29)**. The *R*s values of the different catalyst systems were relatively similar (ranging from 14.31 Ω to 15.96 Ω), and the current densities under comparison were relatively low, resulting in minimal and comparable ohmic losses.

In addition, we further included a performance comparison of the catalysts at the same constant current density, which showed a consistent activity trend. At the same current density of 20 mA cm^{-2}, the urea production rates of CuRu/CS and CuRu/MCHS were 0.964 g h^{-1} g_{cat}^{-1} and 1.583 g h^{-1} g_{cat}^{-1}, respectively (**Fig. S9d**). This confirms that the lack of *i*R compensation in the original data does not alter our conclusions regarding the relative catalytic performance. Meanwhile, we have revised and further discussed this section in the revised manuscript. We sincerely appreciate your valuable comment.

The relevant revisions are presented as follows:

Line 151: "Despite a small absolute offset after *i*R correction, the relative catalyst activity order was preserved, confirming that our comparative conclusions were robust to ohmic drop correction (**Figs. S9c** and **S9d**).**"**

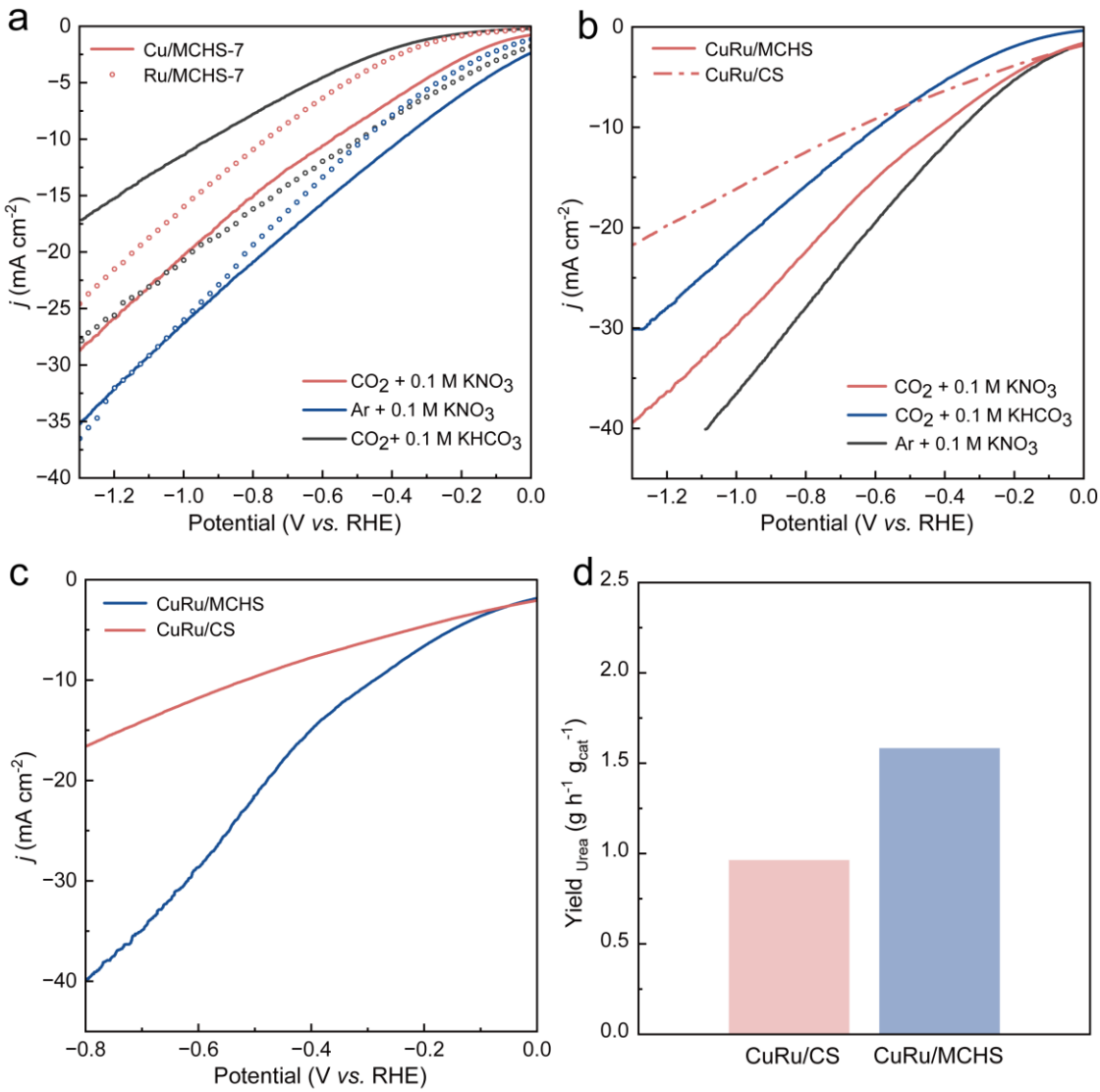

Supplementary Fig. S9| LSV curves of Cu/MCHS, Ru/MCHS, CuRu/CS and CuRu/MCHS at H-cell. a, LSV curves for a Cu/MCHS and Ru/MCHS without *iR* correction. **b**, LSV curves without *iR* correction for CuRu/MCHS and CuRu/CS in the mixture of 0.1 M KNO_3 under CO_2 flow in reference with that in 0.1 M KNO_3 + Ar and 0.1 M $KHCO_3$ + CO_2. The catalyst loading is 0.2 mg cm^{-2}. **c**, The *i*R-corrected LSV curves for CuRu/MCHS and CuRu/CS in the mixture of 0.1 M KNO_3 under CO_2 flow. The solution resistance (*R*s) values of CuRu/MCHS and CuRu/CS were 15.20 Ω and 15.96 Ω, respectively. 85% *i*R compensation was applied. **d**, Urea yield rate of CuRu/MCHS and CuRu/CS in H-cell at 20 mA cm^{-2}. At the same current density of 20 mA cm^{-2}, the urea production rates of CuRu/CS and CuRu/MCHS were 0.964 g h^{-1} g_{cat}^{-1} and 1.583 g h^{-1} g_{cat}^{-1}, respectively.

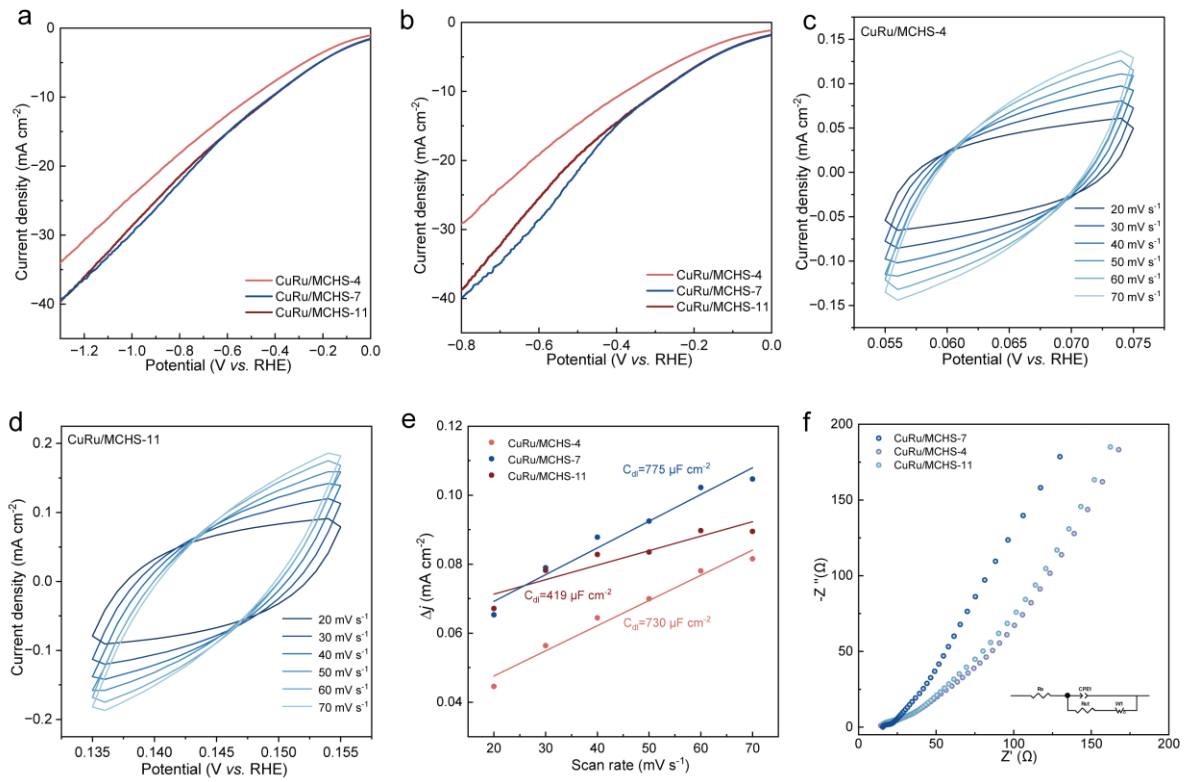

Supplementary Fig. S29| The electrochemical measurements on CuRu/MCHS-4 and CuRu/MCHS-11. **a**, LSV curves and **b** *i*R-corrected LSV curves of electrocatalytic CO_2 and NO_3^- co-reduction by CuRu/MCHS-4, CuRu/MCHS-7 and CuRu/MCHS-11. The *R*s values of CuRu/MCHS-4, CuRu/MCHS-7, and CuRu/MCHS-11 were 14.31 Ω, 15.20 Ω, and 14.39 Ω, respectively. 85% *i*R compensation was applied. Cyclic voltammogram curves of **b** CuRu/MCHS-4 and **c** CuRu/MCHS-11. **d**, *C*dl of corresponding electrocatalysts. **e**, The electrochemical impedance spectra in of CuRu/MCHS-4, CuRu/MCHS-7 and CuRu/MCHS-11 cathodes from 1 M Hz to 0.1 Hz.

5. Although the identification of urea using NMR is valid, the quantification based solely on a urease-based assay could be problematic. This method has been shown to overestimate urea concentrations, particularly in the presence of high ammonium levels (https://doi.org/10.1016/j.cej.2022.139836). Additional quantification techniques or validation would strengthen the conclusions.

Response: Thank you for raising this insightful point for discussion. We have carefully read and referred to the relevant literature you mentioned and sincerely appreciated your comment on the potential limitation of the urease-based assay in overestimating urea concentration under high ammonium levels. We fully agree that accurate quantification is crucial for supporting our conclusions.

To address this concern, we performed additional validation during the revision phase. We re-ran the experiments and quantified urea in the same set of samples using two independent methods: the urease-based UV-Vis assay and high-performance liquid chromatography (HPLC).

In four repeated experiments, the urea production rate quantified by the urease-based UV-Vis method was 4.067 ± 0.227 g h^{-1} g_{cat}^{-1}, while the HPLC method yielded a comparable value of 3.898 ± 0.080 g h^{-1} g_{cat}^{-1}. The close agreement between the two methods confirms that the urease assay did not lead to significant overestimation in our catalytic system. The marginally higher value from the UV-Vis method may be attributed to minor matrix effects or dilution-related uncertainties.

The detailed HPLC methodology and original chromatograms have been included in the Supporting Information. We believe these complementary results firmly validate the accuracy of our urea quantification and reinforce the reliability of the reported catalytic performance.

The relevant revisions are presented as follows:

Line 161: "Urea quantification was cross-validated using both the enzymatic urease and high-performance liquid chromatography (HPLC) methods (**Fig. S11**)[42], with the yields showing strong consistency and a marginal difference. This agreement confirms the accuracy and reliability of the measured urea yields.**"**

Line 564: "High performance liquid chromatography with fluorescence detection (HPLC-FLD) was then used for secondary verification of the urea yield. After the reaction, Ar was continuously purged through the electrolyte for 30 min to remove the dissolved CO_2. In a 40 °C derivatization bath, 0.5 mL of urea standard solution in 0.1 M KNO_3 or the electrolyte were

sequentially mixed with 0.4 mL of methanol solution, 50 μL of xanthydrol solution, and 50 μL of 1% hydrochloric acid solution to undergo a derivatization reaction.”

Supporting Information txt： “The high performance liquid chromatography-fluorescence detection (HPLC-FLD) spectroscopy data were collected using a Waters Acquity Arc HPLC system with Inertsil ODS-4 column (4.6 mm *250 mm, 5 μm). The corresponding mobile phase, column temperature, and detected wavelengths under fluorescence mode were ammonium acetate aqueous solution (0.02 M)–acetonitrile (25:75), 35°C, with excitation at 213 nm and emission at 308 nm.”

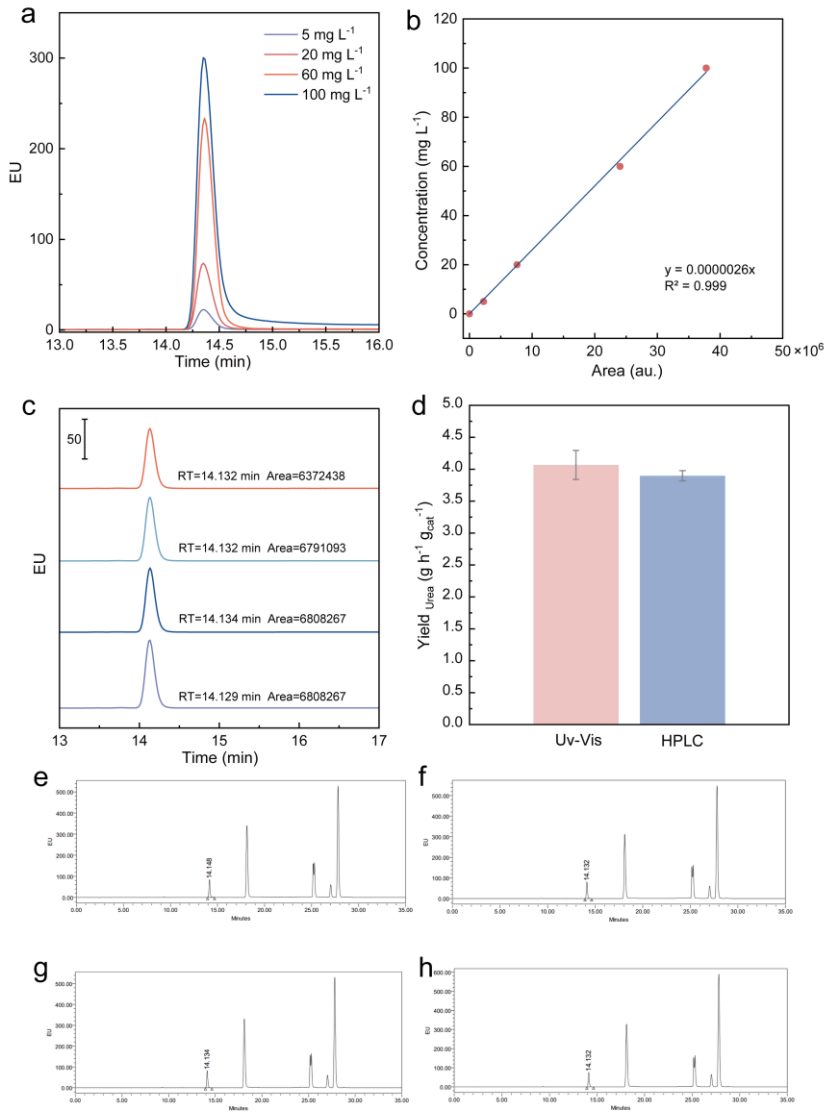

Supplementary Fig. S11| HPLC measurements of urea products. a, HPLC spectra of standard solutions containing different amounts of urea in 0.1 M KNO_3 solution. **b**, The

calibration curve used to determine urea. **c**, HPLC spectra of urea in the liquid product after the reaction. **d**, The urea yield rate of CuRu/MCHS at –1.1 V (vs. RHE) detected by urease dissociation method and HPLC method. The data are presented as mean values ± s.d. (n = 4). **e**-**h**, The original HPLC spectra corresponding to the data.

Newly added references:

42 Huang, Y. *et al*. Unveiling the quantification minefield in electrocatalytic urea synthesis. *Chem. Eng. J.* **453**, 139836 (2023).

6. Electrolysis tests for individual CO_2 and nitrate reduction are essential to isolate and understand side product formation during co-reduction. Currently, faradaic efficiency (FE) values are incomplete—up to 20% unaccounted for in MCHS (Fig. 3b) and up to 40% in CS (Fig. S15). These gaps highlight the need for further product analysis.

Response: We sincerely appreciated your insightful suggestion regarding the importance of comprehensive side product analysis during the co-reduction process. In response, we have expanded our quantification efforts to include additional possible byproducts beyond those initially reported.

In our original analysis, we focused on the main side products commonly reported in urea electrosynthesis: H_2, NH_4^+, NO_2^-, CO, CH_4, and N_2H_4. In those tests, we did not detect the formation of CO and N_2H_4. During the revision, we expanded our detection to include other possible products. Based on previous NMR spectra, no other C–N coupled products or other CO_2RR products were found. We further quantified N_2 using GC, formic acid (HCOOH) by ion chromatography, and hydroxylamine (NH_2OH) by UV-Vis spectroscopy.

The results show that the FE of N_2 was less than 1% for all catalysts. We detected certain amounts of NH_2OH (0.7 ± 0.3% in Cu/MCHS and 1.3 ± 0.2% in CuRu/CS) and HCOOH (10.4 ± 2.2% in Cu/MCHS and 12.5 ± 3.0% in CuRu/CS). Only trace amounts of NH_2OH (0.4 ± 0.1%), N_2 (0.3 ± 0.1%), and HCOOH (0.9 ± 0.1%) were detected in Ru/MCHS, which may be attributed to the stronger hydrogen evolution reaction (HER). We conducted further product analysis for CuRu/MCHS over the full voltage range and updated the product distribution data

accordingly. We acknowledge that the FE of N_2 (0.27%～0.17%), NH_2OH (0.58%～0.27%), and HCOOH (0.79%～0.65%) were all relatively low for CuRu/MCHS.

Although this expanded product analysis has increased the total accounted FE and narrowed the previously noted gaps, a discrepancy of approximately 5%-15% remains at low applied voltages for both CuRu/CS and CuRu/MCHS. This may be attributed to experimental uncertainties such as gas flow variation, headspace gas collection challenges, and analytical measurement tolerances, as also noted in related studies (*ACS Energy Lett.* 9, 1, 323–328 (2024)). The incomplete summation of FEs to 100% is a known challenge in electrochemical systems. In our case, the gap may be attributed to several factors: limitations in product detection (e.g., uncertainties in GC peak integration), an increase in the total gas flow rate between the inlet and outlet, primarily due to the production of gaseous products like H_2, which introduces error when using the inlet flow rate as the basis for FE calculations, and minor gas leakage from the system. These factors collectively contribute to an underestimation of certain FE components.

We have updated the relevant figures and tables with these new results and expanded the discussion on how these findings further elucidate the reaction intermediates and mechanism. We thank you again for this valuable suggestion, which has significantly strengthened the rigor and completeness of our product analysis.

The relevant revisions are presented as follows:

Line 189: "Detailed analysis of the primary products (urea, NH_4^+, NO_2^-, H_2, CH_4, N_2, NH_2OH, and HCOOH) revealed that CuRu/CS exhibited a diversified product distribution (**Fig. S15** and **Fig. S16**)."

Line 193: "Moreover, the formation tendency of the byproduct HCOOH was markedly suppressed, as evidenced by a decrease in FE from $12.5 \pm 3.0\%$ to $0.7 \pm 0.1\%$ at –1.1 V (vs. RHE). Within the tested potential range, CuRu/MCHS produced only trace amounts of N_2, NH_2OH, and HCOOH, with FEs all below 1%. Further evaluation of the performance of Cu/MCHS, Ru/MCHS, and CuRu/MCHS with varying molar ratios between Cu and Ru

indicated that Ru/MCHS showed a strong tendency for H_2 production, while Cu/MCHS favoured NO_2^- (26.9 ± 1.1%) and HCOOH (10.4 ± 2.2%) generation (**Fig. S17**).**"**

Line 256: "The limited hydrogenation of CO_2 to *COOH on CuRu/MCHS also correlates with the suppressed formation of HCOOH.**"**

Line 577: "The quantification of NH_2OH was based in its reduction of Fe^{3+} to Fe^{2+} which then forms an orange complex with 1,10-phenanthroline. 1.2 mL of a 1 M aqueous acetate buffer (0.048 M sodium acetate with 0.952 M glacial acetic acid), 60 μL of 15 mM ammonium iron (III) sulfate dodecahydrate aqueous solution and 0.6 mL of 5 mM aqueous 1,10-phenanthroline solution were added into 1.2 mL of the electrolysis solution. The mixture was allowed to stand for 50 min before absorbance measurement at 510.5 nm using a UV-Vis. HCOOH was quantitatively analyzed by ion chromatography (IC).**"**

Supporting Information txt：**"**The ion chromatography (IC) data were collected in Dionex Aquion (Thermofisher Scientific).**"**

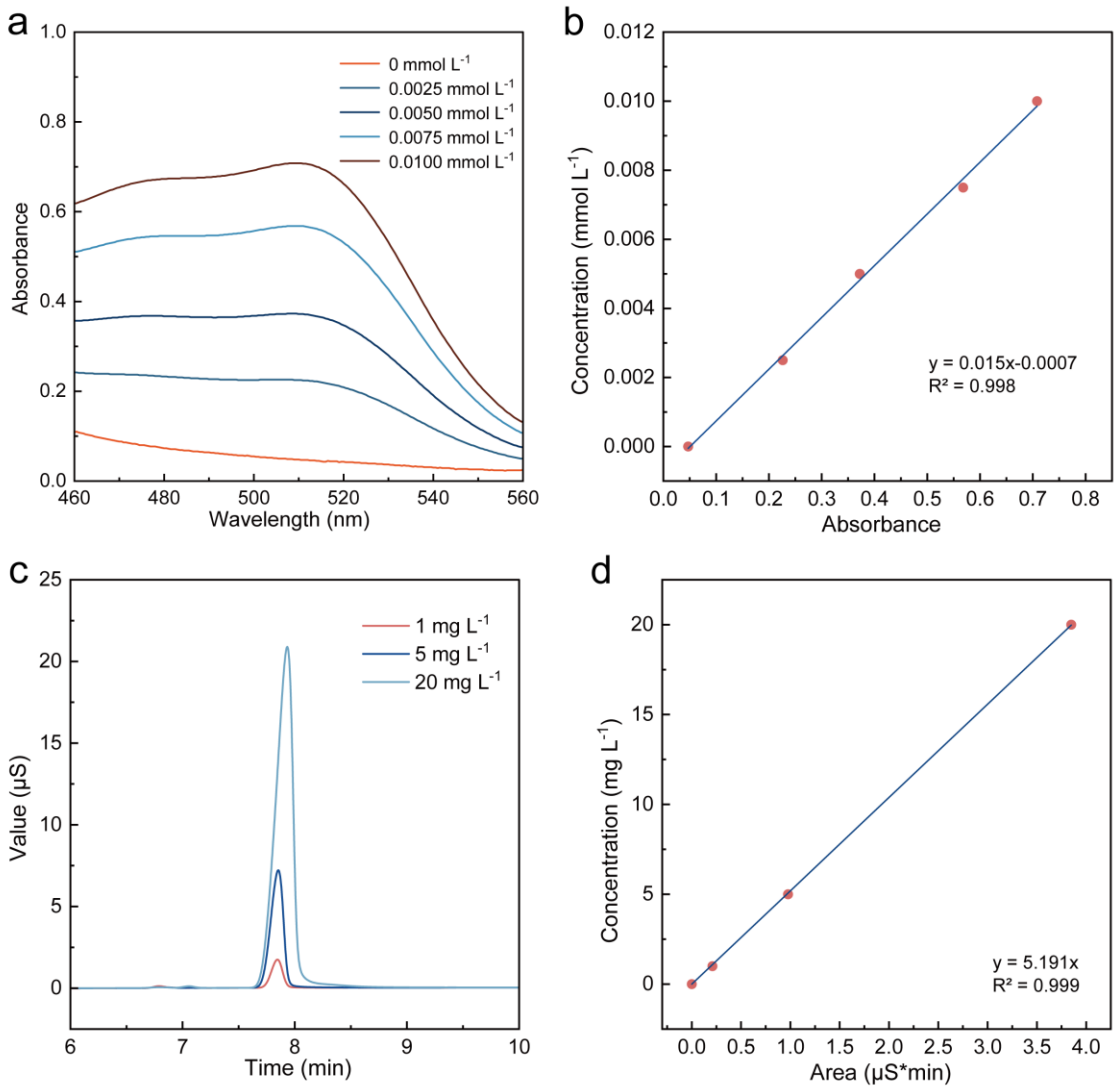

Supplementary Fig. S16| Measurements of the concentrations of NH_2OH and HCOOH. **a,** UV-vis spectra of various NH_2OH standard solution in 0.1 M KNO_3. **b**, The calibration curve for quantification of NH_2OH indicates good linear relation of absorbance with NH_2OH concentration. **c**, IC spectra of various HCOOH standard solution in 0.1 M KNO_3. **d**, The calibration curve for HCOOH quantification indicates good linear relationship with concentration.

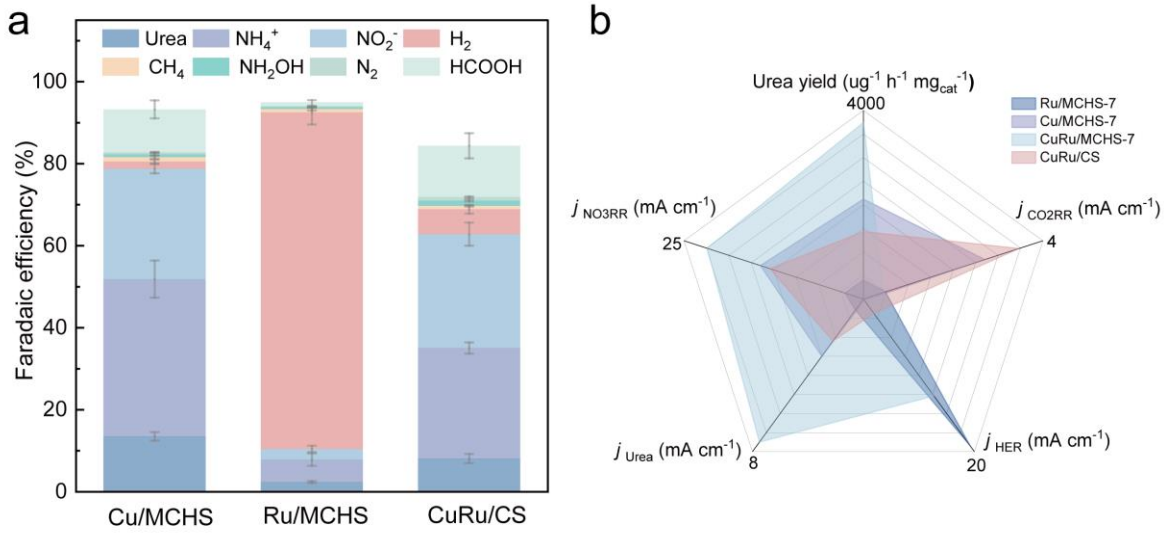

Supplementary Fig. S17| Performance of electrosynthesis of urea. a, FEs of CH_4, H_2, NO_2^-, NH_4^+, NH_2OH, N_2, HCOOH and urea of Cu/MCHS, Ru/MCHS and CuRu/CS as electrocatalyst at the potential of –1.1 V (vs. RHE). CO and N_2H_4 by-products were not detected under any conditions. **b**, Comparison of various properties of CuRu/MCHS, CuRu/CS, Cu/MCHS and Ru/MCHS catalysts.

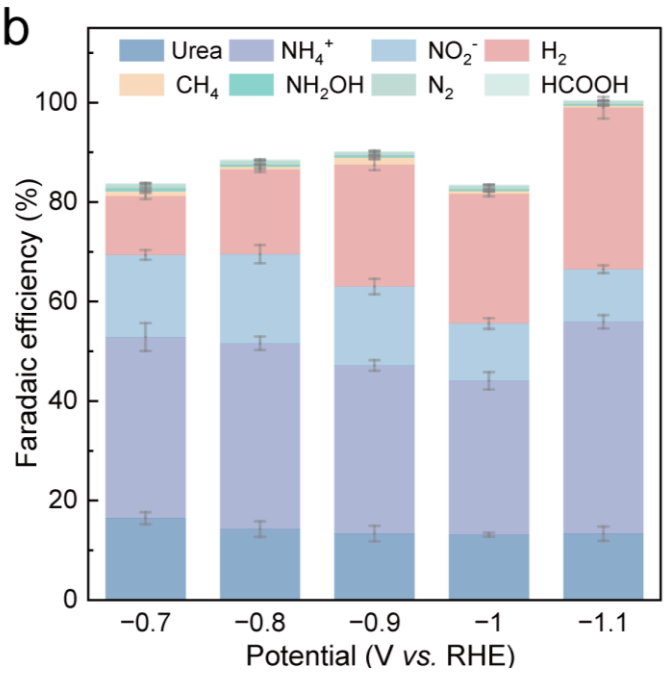

Fig. 3| Urea electrosynthesis performance of nano-confined and non-confined based electrocatalyst. b, Potential-dependent FEs of primary products for CuRu/MCHS assessed in 0.1 M KNO_3 + CO_2.

7. The reasoning behind electrolyte selection should be better explained. For instance, why is potassium bicarbonate used only in the absence of nitrate? As bicarbonate can buffer CO_2 availability, this discrepancy could affect the comparability of results under different reaction conditions.

Response: Thank you for noticing this detail, which was indeed a factor we carefully considered during our experiments. **Firstly**, in CO_2 reduction reactions (CO_2RR), $KHCO_3$ was one of the most commonly used electrolytes, as the equilibrium between HCO_3^- and dissolved CO_2 ensured sufficient CO_2 supply while also providing a buffered environment. Therefore, we used 0.1 M $KHCO_3$ as the electrolyte when we evaluated solo CO_2RR activity. Due to the difference in conductivity between 0.1 M $KHCO_3$ and 0.1 M KNO_3 electrolytes, we did not compare the CO_2RR and C–N co-reduction activities of the same catalyst under these two conditions. In our work, we only focused on comparing different catalysts within the CO_2RR system.

Secondly, in recent literature on CO_2–NO_3^- co-reduction, an increasing number of studies have omitted the additional use of 0.1 M $KHCO_3$ as an electrolyte component (*Nat. Sustain.* 4, 868–876 (2021); *Nat. Synth.* 3, 794–796 (2024)). Some studies have suggested that using 0.1 M KNO_3 alone provides a more appropriate CO_2-to-NO_3^- ratio, better matching the stoichiometric ratio of carbon and nitrogen atoms in urea, which is beneficial for achieving higher urea yield and FE (*Nat. Commun.* 14, 4491 (2023)). **Moreover**, the role of electrolytes in influencing reaction intermediates has not yet been fully established. The effects of electrolyte concentrations on the C–N coupling process itself also remain to be clarified (*Nat. Rev. Chem.* 6, 303–319 (2022)). **In our study**, $KHCO_3$ was intentionally avoided in co-reduction experiments involving nitrate, in order to minimize the introduction of additional carbon sources and prevent potential interference with carbon-related reaction pathways.

Your suggestion is of great research value, and we also acknowledge that the choice of electrolyte can influence catalytic activity. To address this, we have conducted additional electrosynthesis experiments using an electrolyte composed of 0.1 M $KHCO_3$ + 0.1 M KNO_3

at –1.1 V vs. RHE. Under these conditions, the urea yield and FE were 1.867 ± 0.138 g h^{-1} g_{cat}^{-1} and 9.9 ± 1.6%, respectively (**Fig. S38)**. This performance was noticeably lower compared to that using 0.1 M KNO_3 alone (3.74 ± 0.25 g h^{-1} g_{cat}^{-1} and 13.3 ± 1.4%) as the electrolyte. This difference may be attributed to the presence of HCO_3^-, which could interfere with C–N bond formation involving *OCO intermediates or compete for catalytic active sites. Furthermore, the addition of 0.1 M $KHCO_3$ raised the pH of the electrolyte from ~4.1 (CO_2-saturated 0.1 M KNO_3 solution) to ~6.8 (0.1 M $KHCO_3$ + 0.1 M KNO_3), which may also influence the reaction environment.

Our study was designed to optimize each single-reduction system individually and to replicate their typical reaction conditions as faithfully as possible. At the same time, we aimed to avoid introducing non-target reaction pathways in the co-reduction system, for example, the differing effects of HCO_3^- and CO_2 on C–N bond formation. Therefore, in this work, $KHCO_3$ was used only in the standalone CO_2RR experiments. We sincerely appreciate your suggestion, which has helped us further clarify the role of the electrolyte.

The relevant revisions are presented as follows:

Line 524: "The introduction of an additional carbon source (0.1 M $KHCO_3$ + 0.1 M KNO_3) decreased both the urea yield and FE compared to 0.1 M KNO_3 alone (**Fig. S38**). Therefore, considering factors such as pH, the stoichiometric ratio of carbon to nitrogen atoms, and avoid introducing non-target reaction pathways, 0.1 M KNO_3 was selected as the electrolyte for the co-reduction of CO_2 and NO_3^-. The 0.1 M KNO_3 was applied to electrocatalysis of sole NO_3^- reduction. The 0.1 M $KHCO_3$ was applied to electrocatalysis of sole CO_2 reduction.**"**

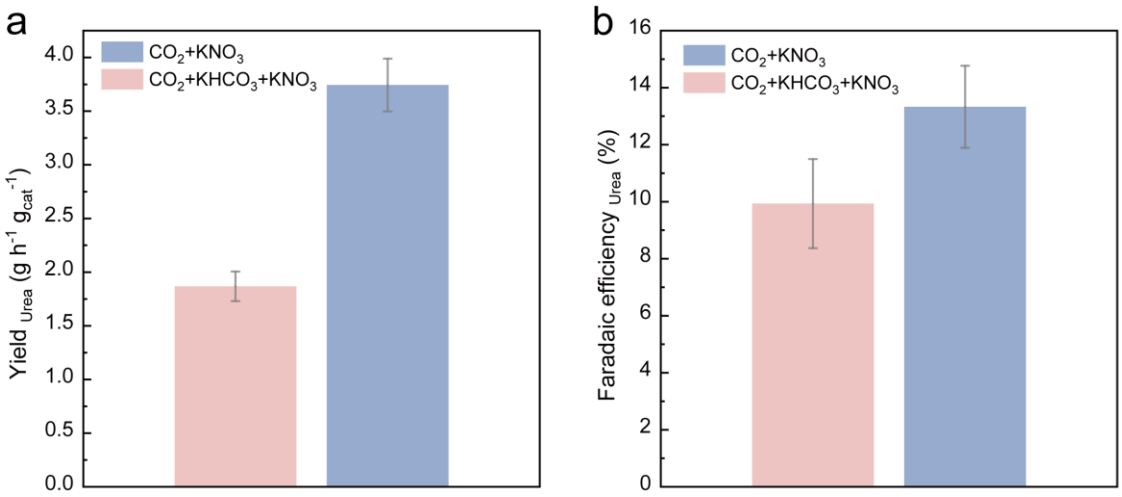

Supplementary Fig. S38| Yield rate and FE of CuRu/MCHS in different electrolytes. a, Urea yield rate and **b** FE of CuRu/MCHS at –1.1 V (vs. RHE) in CO_2-saturated 0.1 M KNO_3 and 0.1 M $KHCO_3$ + 0.1 M KNO_3 electrolytes.

8. The authors should specify the Cu:Ru ratios used in Figs. 3a and 3b and explain the omission of the 24:1 ratio from Fig. 3c.

Response: Thank you for your valuable comment. To clarify, the data for the $Cu_{24}Ru_1$/MCHS catalyst (i.e., CuRu/MCHS with a 24:1 molar ratio) were originally included in **Figs. 3a** and **3b** but were not displayed in **Fig. 3c**. In response to your comment, we have now incorporated the $Cu_{24}Ru_1$/MCHS performance data into **Fig. 3c** to allow for a more complete and direct comparison across all compositions. The corresponding figure caption has also been updated to explicitly indicate the Cu:Ru ratio used in each case.

The relevant revisions are presented as follows:

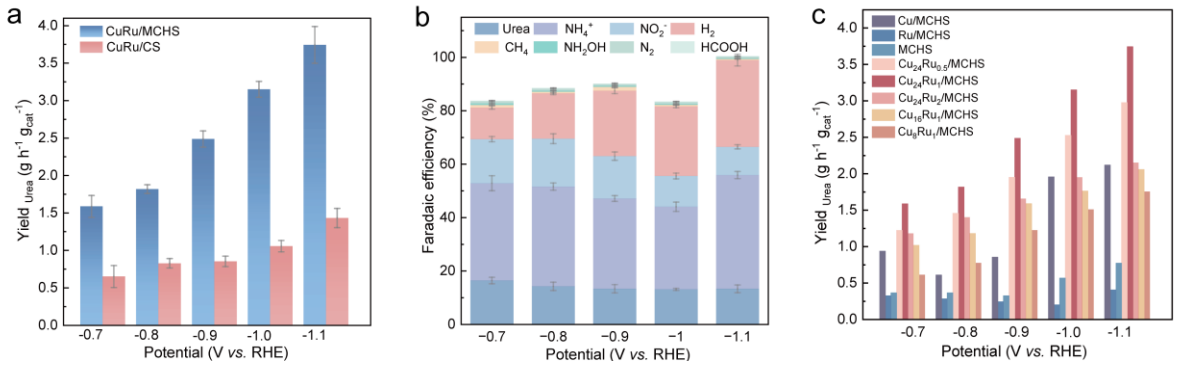

Fig. 3| Urea electrosynthesis performance of nano-confined and non-confined based electrocatalyst. a, Urea yield rate of CuRu/MCHS and CuRu/CS at different potentials. **b**, Potential-dependent FEs of primary products for Cur/MCHS assessed in 0.1 M KNO_3 + CO_2. The proportion of Cu to Ru used in preparing CuRu/MCHS and CuRu/CS was fixed at a molar ratio of 24:1 ($Cu_{24}Ru_1$/MCHS). **c**, Comparison of the performance for urea electrosynthesis by Cu/MCHS, Ru/MCHS, MCHS, $Cu_{24}Ru_2$/MCHS, $Cu_{24}Ru_1$/MCHS, $Cu_{24}Ru_{0.5}$/MCHS, $Cu_{16}Ru_1$/MCHS and Cu_8Ru_1/MCHS as electrocatalyst at the potentials of –0.7, –0.8, –0.9, –1.0 and –1.1 V (vs. RHE).

*9. From Fig. 3, it is evident that ammonium is the dominant product in terms of FE. However, in lines 213–215, the ATR-SEIRAS spectra are interpreted to suggest that hydrogenation to form *NH_2 is suppressed during CO_2–NO_3^- co-reduction. This interpretation appears contradictory, given the high ammonium production observed. The authors should reconcile these findings.*

Response: We appreciate your insightful observation regarding the relationship between the ATR-SEIRAS interpretation and the observed ammonium production. The apparent contradiction can be reconciled by considering the distinct temporal scales and detection sensitivities of the two analytical methods.

The ATR-SEIRAS spectra capture real-time surface intermediates under operando conditions. While characteristic *NH_2 peaks were indeed observed for CuRu/MCHS (as visible in **Fig. 4b**, shown below), their intensity was relatively lower than that on CuRu/CS, indicating that *NH_2 accumulation is kinetically less favored relative to the competing *OCONO coupling pathway under co-reduction conditions. This does not imply complete suppression of the hydrogenation pathway, but rather reflects a lower steady-state surface concentration of *NH_2.

Conversely, the high FE of NH_4^+ represents the cumulative product distribution over the entire electrolysis period. Once formed, even a small amount of *NH_2 can be rapidly protonated to NH_4^+. This rapid consumption limits its detectable presence on the surface at any given moment, while still contributing significantly to the final NH_4^+ product over time.

We have revised the manuscript to clarify that while the *OCONO pathway is favored on CuRu/MCHS, the hydrogenation pathway remains active but exhibits different intermediate retention kinetics compared to CuRu/CS. Thank you for highlighting this point, which has

helped us provide a more precise interpretation of our spectroscopic and product distribution data

The relevant revisions are presented as follows:

Line 251: "Notably, characteristic vibrational peaks for *CO (2050 cm^{-1})[16] in CO_2RR and *NH_2 (3345 and 1177 cm^{-1})[54,55] in NO_3RR were markedly attenuated during CO_2 and NO_3^- co-electroreduction, though a weak but observable *NH_2 signal was still detected on CuRu/MCHS (**Fig. 4b**). This suggests that the pathways of CO_2 → *COOH → *CO was suppressed during C–N coupling, as further confirmed by the absence of a *COOH signal on CuRu/MCHS (**Fig. 4c**). The limited hydrogenation of CO_2 to *COOH on CuRu/MCHS also correlates with the suppressed formation of HCOOH. In contrast, the CuRu/CS catalyst exhibited distinct signals of *COOH (1395 cm^{-1})[56] and *NH_2 (3345 and 1170 cm^{-1}) intermediates (**Fig. 4d**). As the potential increased from −0.1 V to −1.5 V (vs. RHE), *NH_2 species were gradually consumed while *COOH intermediates initially formed and progressively accumulated. This was in accordance with the appearance of C–N and N–C–N signals, yet with much lower intensities than CuRu/MCHS (**Fig. 4e**). The absence of *NO and *OCO signals on CuRu/CS indicated their rapid hydrogenation into *NH_2 and *COOH, hindering the effective retention of pre-hydrogenation intermediates. Conversely, in CuRu/MCHS, the *NO species generated during NO_3^- reduction were preserved, enabling earlier coupling with *OCO. Note that the *NH_2 generated were rapidly protonated to NH_4^+, which limited the steady-state surface concentration of *NH_2 and thus its spectral intensity, despite the significant NH_4^+ product accumulation observed over the full electrolysis period."

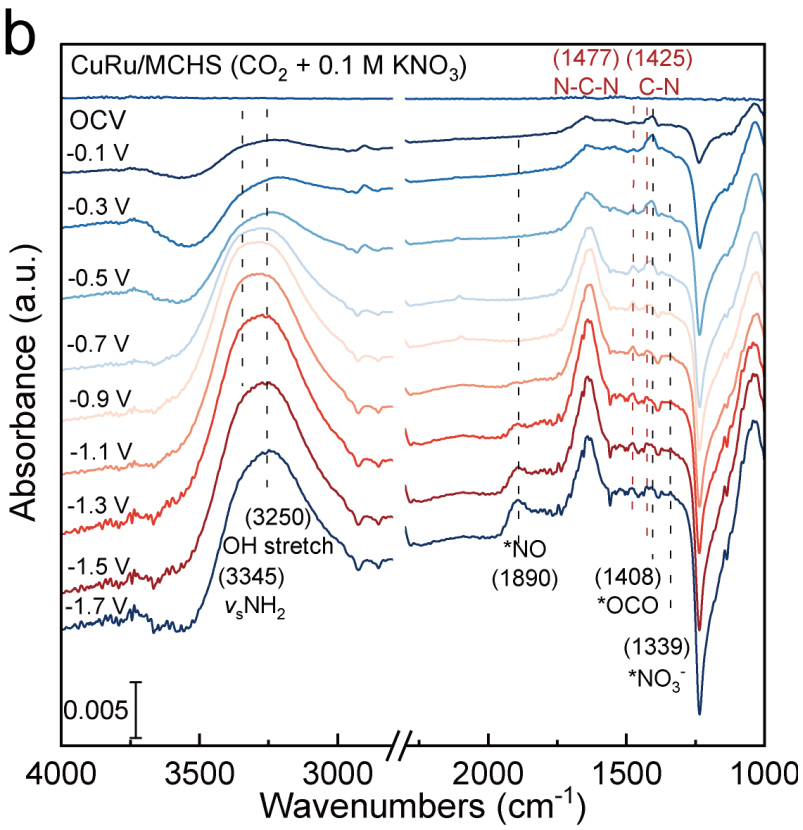

Fig. 4| Mechanistic study of CuRu/MCHS and CuRu/CS. b-c, ATR- SEIRAS spectra of CuRu/MCHS recorded from the open-circuit state to –1.7 V (vs. RHE) in a 0.1 M KNO_3 electrolyte with CO_2 bubbling between **b** 1000–4000 cm^{-1} and **c** 1350–1500 cm^{-1}.

10. Reporting the initial and final pH values for electrolysis experiments is important. Changes in pH due to reduction reactions can influence both the reaction environment and the calibration of the applied potential vs. RHE.

Response: We thank you for this valuable suggestion. We agree that monitoring pH evolution during electrolysis is essential, as it influences both the reaction environment and the accurate calibration of applied potential versus RHE. In the revised manuscript, we have now included both initial and final pH values for experiments. The initial pH was 7.6 in 0.1 M KNO_3 electrolyte and 4.1 in CO_2-saturated 0.1 M KNO_3 solution. After electrolysis, the final pH measured was 4.9 for CuRu/MCHS and 4.7 for CuRu/CS, indicating a moderate increase. This pH rise is primarily attributed to the substantial consumption of protons (H^+) during the

reduction processes, such as NO_3^-/CO_2 reductions and HER. The continuous CO_2 bubbling provided a buffering effect that helped mitigate a more drastic pH increase. All catalytic evaluations were conducted under identical initial pH conditions, with only minor variations observed in post-reaction pH across different catalysts. These data have been added to the Supporting Information (**Fig. S18**).

The relevant revisions are presented as follows:

Line 213: "The electrolyte pH exhibited only a moderate increase from 4.1 to 4.9 for CuRu/MCHS and to 4.7 for CuRu/CS after electrolysis. This limited change indicates that the substantial H^+ consumption was effectively mitigated by the buffering capacity of the CO_2-saturated solution (**Fig. S18**)."

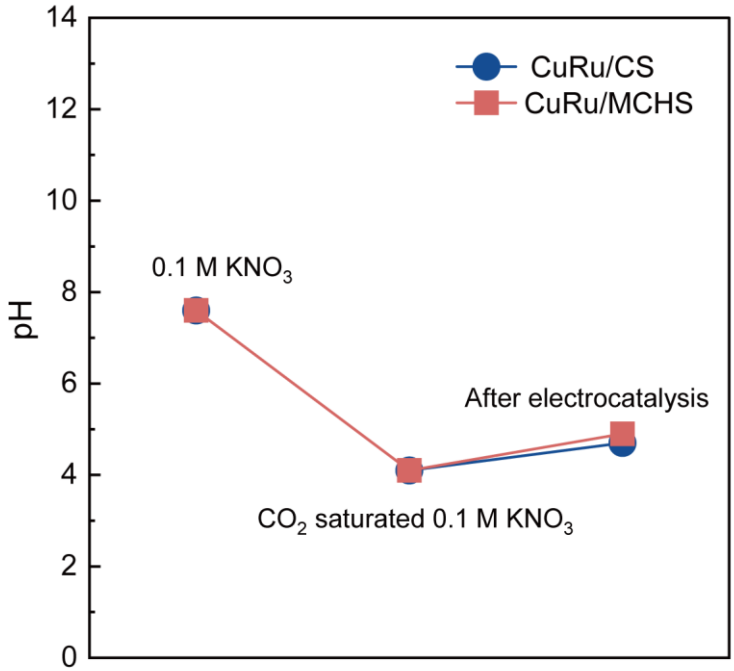

Supplementary Fig. S18| The pH variation plots of CuRu/MCHS and CuRu/CS before and after the electrocatalysis.

11. In lines 281–285, the authors suggest that a pore size of 7 nm optimizes urea synthesis, but the mechanistic basis for this observation is not discussed. Possible explanations (e.g., optimal

confinement effects, mass transport considerations, or surface accessibility) should be explored.

Response: We thank you for this insightful comment. The optimal performance at the 7 nm pore size indeed represents a key finding, and we agree that elucidating its mechanistic basis is crucial. Based on our experimental and simulation results, we propose that the 7 nm pore architecture achieves an optimal balance between mass transport and confinement effects, which collectively enhance C–N coupling efficiency. This can be explained by the following aspects:

1. Balanced reactant flux and intermediate retention: Our FEM (**Fig. 6d-f**) reveals that the 7 nm pore size offers a superior compromise. Compared to the 4 nm pores, it allows for a higher influx of reactants (CO_2 and NO_3^-), mitigating diffusion limitations. Simultaneously, compared to the 11 nm pores, it provides a stronger confinement effect, which is crucial for retaining the key reactive intermediates (*H, *NO, and *OCO) within the cavity, thereby increasing their local concentration and probability of successful C–N coupling.

2. Optimal *H availability and management: The EPR results (**Fig. 6c**) indicate that the CuRu/MCHS-7 catalyst generates the most abundant *H species. More importantly, the FEM simulations (**Fig. 6e**) show that the 7 nm pore structure is most effective at utilizing the generated *H for the urea formation pathway, rather than losing it to H_2 evolution or diverting it to excessive NH_4^+ production (as seen in the product distribution of **Fig. 5i**). This optimal *H management is critical for driving the hydrogenation steps in the *OCONO pathway.

3. Spatial compatibility with reaction intermediates: The pore size is comparable to the diffusion length scales of the critical intermediates. A 7 nm channel is sufficiently large to accommodate the transport of reactant molecules yet sufficiently constrained to prolong the residence time of the *NO and *OCO intermediates, facilitating their encounter and coupling. The optimal nano-confinement effect in pore size of 7 nm simultaneously ensured the fast CO_2/NO_3^- inflow from the exterior into the interior of the cavity and the retention of the intermediates of *H and *NO within the cavity, thus leading to a highest urea selectivity and production rate in CuRu/MCHS-7.

In summary, the 7 nm pore is not merely a geometric optimum but represents a kinetic optimum where the rates of reactant supply, intermediate coupling, and product retention are best matched. We have now incorporated this detailed mechanistic discussion into the revised manuscript (in the section discussing **Fig. 6g**) to clarify the underlying reasons for the observed volcano-shaped relationship.

Line 435: "Overall, the 7 nm pore architecture represents a kinetic optimum, arising from a synergistic balance among three pivotal factors (**Fig. 6g**). First, it established an optimal balance between mass transport and confinement. The 7 nm pores achieved the best compromise between efficient CO_2/NO_3^- influx and effective retention of key intermediates (*H and *NO), avoiding the diffusion limitations observed in the 4 nm pores and the rapid intermediate leakage that occurred in the 11 nm pores. Second, it enabled highly efficient utilization of intermediates. The moderate confinement within the 7 nm cavities maintained a high local concentration of reactive species, maximized the generation and utilization of *H species (as confirmed by EPR results), and spatially confined them to preferentially participate in the hydrogenation steps of the *OCONO pathway, rather than being consumed by H_2 evolution or excessive NH_4^+ formation. Third, it realized a synergistic kinetic effect of confinement. The 7 nm structure provided a kinetic optimum by harmonizing reactant supply, intermediate stabilization, and product diffusion, thereby delivering the highest urea selectivity and production rate. Collectively, this multi-scale regulation enhances the local availability of reactive species, lowers the kinetic barriers for C–N coupling, and steers the reaction pathway toward urea formation, demonstrating that precise pore-size engineering provides a powerful lever for optimizing complex electrocatalytic processes.**"**

*12. In Fig. 6a, the authors show a significant decrease in urea yield when switching from H_2O to D_2O, indicating that C–N coupling may involve *H. The authors briefly suggest this in line 615, but the mechanistic implications deserve further elaboration.*

Response: We sincerely thank you for this insightful comment, which helps us uncover the deeper mechanistic role of *H in the C–N coupling process. The significant kinetic isotope

effect (KIE) observed in D_2O (**Fig. 6a**) confirms that proton-coupled electron transfer (PCET) steps are integral to the rate-determining process of urea formation. In response to your suggestion, we have substantially expanded the mechanistic discussion in the revised manuscript by integrating our DFT calculations with the experimental KIE results.

Our DFT analysis reveals that while the initial OCO–NO coupling presents a substantial energy barrier (0.79 eV), the subsequent hydrogenation steps along the *OCONO pathway proceed through more favorable energy landscapes. Specifically, the hydrogenation of key intermediates such as *OCONO to *OCONOH, and eventually to urea, involves sequential *H incorporation with lower activation barriers. This indicates that the presence of *H is essential not only in the final product formation but also in stabilizing the reaction pathway after the initial C–N bond formation. The pronounced KIE strongly suggests that one or more of these hydrogenation steps, likely the protonation of *N–O or *C–O moieties in the *OCONO-derived intermediates, contributes kinetically to the overall reaction rate. The nano-confinement environment in CuRu/MCHS, as supported by EPR and FEM, optimizes the local *H availability and spatial distribution, thereby facilitating these critical PCET steps and steering the selectivity toward urea over side products.

Thank you again for pushing us to provide a more mechanistic perspective. We have revised the manuscript to clarify how the *H-mediated hydrogenation steps are intricately coupled to the C–N bond formation energetics, underscoring the synergy between nano-confinement and reaction kinetics.

The relevant revisions are presented as follows:

Line 376: "To confirm the role of *H in urea synthesis, the catholyte was replaced by D_2O[63]. The urea yield of CuRu/MCHS-7 decreased by 72% from 3.74 ± 0.25 to 1.00 ± 0.19 g h^{-1} g_{cat}^{-1} at –1.1 V (vs. RHE) (**Fig. 6a** and **Fig. S32**), yielding a kinetic isotope effect (KIE, defined as the ratio of urea formation rates in H_2O vs D_2O) value of 3.6. This significant KIE (>1) confirms that proton-transfer events are involved in the rate-determining step of the C–N coupling mechanism[64]. Combined with our DFT calculations, we propose that while the initial OCO–NO coupling presents a substantial energy barrier, the subsequent hydrogenation steps

along the *OCONO pathway involve sequential *H incorporation through PCET processes (**Fig. 6b**)[65,66]. The observed KIE likely arises from one or more of these PCET steps, where *H acts as a crucial hydrogen source for stabilizing key intermediates such as *OCONO and facilitating its conversion to urea. This interpretation aligns with the role of *H as an essential participant in the hydrogenation of N–O and C–O moieties during the later stages of the C–N coupling pathway, rather than being limited solely to the initial Volmer step.**"**

Newly added references:

64 Liu, Y. & McCrory, C. C. L. Modulating the mechanism of electrocatalytic CO_2 reduction by cobalt phthalocyanine through polymer coordination and encapsulation. *Nat. Commun.* **10**, 1683 (2019).

65 Feng, J. *et al.* Modulating adsorbed hydrogen drives electrochemical CO_2-to-C_2 products. *Nat. Commun.* **14**, 4615 (2023).

66 Zhao, Z. *et al.* Dynamical barrier and isotope effects in the simplest substitution reaction via Walden inversion mechanism. *Nat. Commun.* **8**, 14506 (2017).

Overall, this study proposes a promising strategy for improving urea production via the co-reduction of CO_2 and nitrate, and the integration of nanoconfinement principles with bifunctional metal catalysts is noteworthy. However, the manuscript would benefit significantly from clearer interpretation of characterization data, consistent reporting of electrochemical metrics, and a more detailed mechanistic discussion. Addressing these concerns—either through improved explanation or additional experimentation—will strengthen the scientific rigor and impact of the work.

Response: We sincerely thank you for your positive assessment of our work and for acknowledging the significance of combining nano-confinement design with bimetallic catalysts in urea electrosynthesis. We are also grateful for the constructive suggestions concerning data interpretation, consistency in electrochemical reporting, and deeper mechanistic discussion. In response, we have carefully addressed each of the points raised, through additional experiments, data re-analysis, and expanded discussions in the revised manuscript. These revisions have substantially enhanced the scientific rigor and clarity of our study. We truly appreciate your insightful comments and guidance throughout the review process.

Reviewer 3

Comments: *The manuscript entitling "Nano-confinement Engineering Boosts C–N Coupling for Urea Electrosynthesis" presents an in-depth study on the electrosynthesis of urea via the co-reduction of CO_2 and nitrate using a nano-confined CuRu bimetallic catalyst within mesoporous carbon hollow spheres (MCHS). The authors demonstrate how nano-confinement architecture significantly improves urea yield, selectivity, and reaction kinetics by altering intermediate species and enhancing transport properties. The work combines comprehensive experimental characterization with in situ spectroscopies and DFT simulations to elucidate the mechanism, presenting an excellent and timely research. With minor clarification on mechanisms, catalyst optimization, and reproducibility details, the manuscript will be suitable for publication in a high-impact journal like Nature Communications.*

Response: We sincerely thank you for your thorough evaluation of our work and for your positive assessment of its significance and timeliness. We are particularly grateful for the acknowledgment that our study combines comprehensive experimentation with theoretical analysis to elucidate the mechanism. We have carefully addressed all the points raised regarding mechanistic clarification, catalyst optimization, and reproducibility details in the revised manuscript. Below, we provide a point-by-point response to each specific comment, with all corresponding revisions clearly indicated in the main text and supporting information. We believe these revisions have significantly strengthened the manuscript and thank you again for their insightful guidance.

*1. While the switching from *COOH–*NH_2 to *OCO–*NO is discussed, a clearer visual or tabulated comparison of energy barriers and reaction paths between confined and non-confined catalysts would enhance readability. The authors are requested to go through the following manuscript: doi.org/10.1021/acs.jpclett.1c03242.*

Response: Thank you for the helpful suggestion. We agree that a more direct comparison between confined and non-confined catalysts would improve the clarity of our mechanistic analysis. We have also consulted the recommended reference and and used it as guidance to prepare the relevant figures and tables.

Although the **Fig. 4h** was intentionally used to visualize the reaction path difference between confined and non-confined catalysts, we have added a more explicit visual representation of the reaction pathway transitions between the confined and non-confined catalysts in the revised manuscript (**Fig. S26**). In addition, we have incorporated a tabulated comparison of the associated energy barriers for the two pathways (**Table S11**). We believe that these additions substantially improve the clarity and depth of the mechanistic interpretation.

The relevant revisions are presented as follows:

Line 316: "ATR-SEIRAS and DFT collectively elucidated that with the nano-confined structure, CuRu/MCHS enabled earlier C–N coupling through the *OCONO pathway (**Fig. 4h**), eliminating four N-hydrogenation and one C-hydrogenation steps versus the *$COOHNH_2$ pathway and suppressing byproduct formation (**Fig. S26**)[58-61]**."**

Line 288: "In contrast, the *$COOHNH_2$ path exhibited a smaller energy barrier of 0.64 eV during the first C–N coupling step (*COOH+*NH_2 → *$COOHNH_2$), yet with a much longer reaction path from *OCO and *NO (**Table S10** and **Table S11**)."

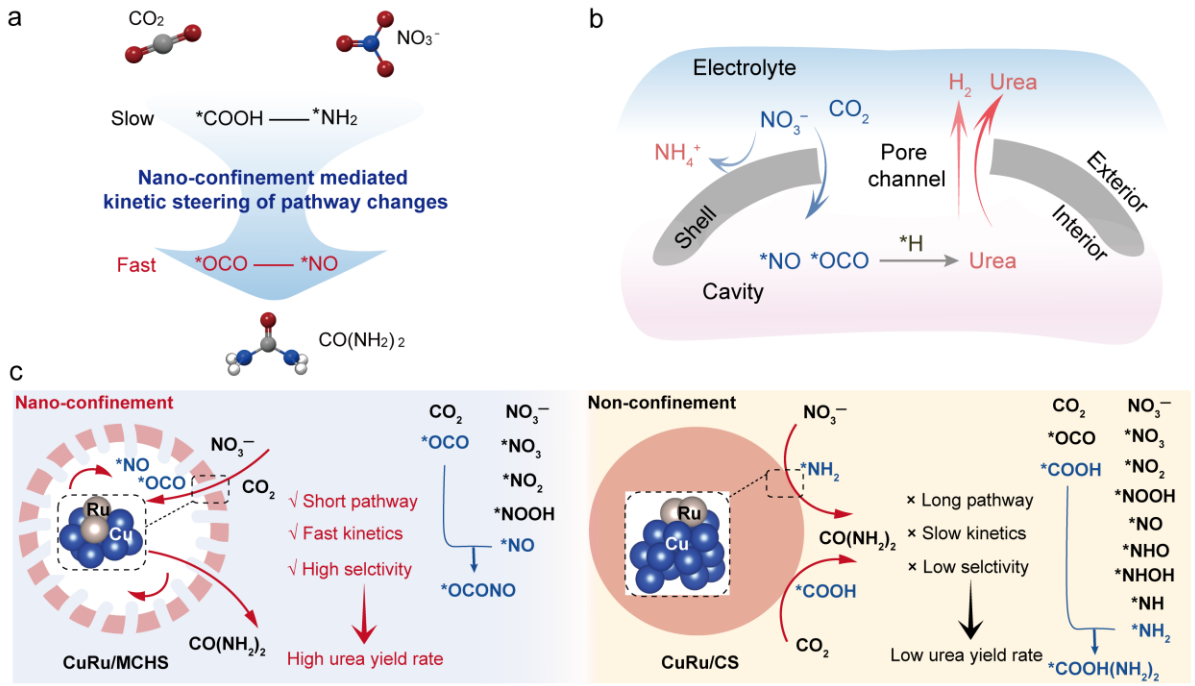

Supplementary Fig. S26| Schematic illustration of reaction pathway conversion in CuRu/MCHS and CuRu/CS. Conceptual diagram of the **a** reaction comparison and **b**

pathway transition between nano-confined and non-confined catalysts. **c**, The diffusion and transformation of reactants and products within the cavities and pores of CuRu/MCHS.

Supplementary Table S10| The calculated ΔE, ΔE_{ZPE} and $T\Delta S$ of various species along the reaction pathways for urea synthesis on the CuRu model .

Species	ΔE (eV)	ΔE_{ZPE} (eV)	$T\Delta S$ (eV)
HNO_3	-28.59	0.71	0.35
$*CO_2$	-1111.39	0.28	0.35
*COOH	-1115.20	0.60	0.38
$*CO_2NO$	-1126.15	0.53	0.45
$*CO_2NHO$	-1131.06	0.88	0.46
$*CO_2NHOH$	-1134.75	1.19	0.51
$*CO_2NH$	-1125.32	0.76	0.34
$*CO_2NH_2$	-1129.45	1.11	0.41
$*COOHNH_2$	-1132.78	1.39	0.51
$*CONH_2$	-1120.86	0.94	0.36
$*ONCONH_2$	-1135.95	1.23	0.41
$*CO(NH_2)$	-1137.96	1.77	0.44
$*CO_2$+*NO	-1126.71	0.50	0.65
$*CO_2$+*NHO	-1131.21	0.79	0.70
$*CO_2$+*NHOH	-1135.58	1.09	0.71
$*CO_2$+*NH	-1125.76	0.66	0.49
$*CO_2$+$*NH_2$	-1130.19	0.98	0.52
*COOH+$*NH_2$	-1133.12	1.27	0.68

Supplementary Table S11| The calculated free energy barriers of *COOH-NH_2 and *OCO-NO pathways for urea synthesis on the CuRu model .

Reaction coordinates	ΔG (eV)
$*CO_2$+*NO → $*CO_2NO$	+0.79
$*CO_2NH_2$ → $*CO_2NO$	+0.33
$*CO_2$+$*NH_2$ → *COOH+$*NH_2$	+0.67
*COOH+$*NH_2$ →$*COOHNH_2$	+0.64

Newly added references:

61 Roy, P., Pramanik, A. & Sarkar, P. Dual-silicon-doped graphitic carbon nitride sheet: An efficient metal-free electrocatalyst for urea synthesis. *J. Phys. Chem. Lett.* 12, 10837-10844 (2021).

2. The Ru loading is extremely low (Cu:Ru = 24:1). The rationale behind this choice and its optimization deserves further discussion.

Response: We thank you for raising this important point regarding the Ru loading in our catalyst design. The selection of the Cu:Ru = 24:1 molar ratio was indeed intentional and carefully optimized, driven by the goal of maximizing both catalytic performance and atomic efficiency. As shown in **Fig. 3c**, we systematically evaluated catalysts with fixed Cu loading but varying Ru contents ($Cu_{24}Ru_2$/MCHS, $Cu_{24}Ru_1$/MCHS, $Cu_{24}Ru_{0.5}$/MCHS). The urea yield exhibited a distinct volcano-type dependence on Ru content, with $Cu_{24}Ru_1$/MCHS (i.e., Cu:Ru = 24:1) demonstrating the highest production rate. To further substantiate this optimum, we have now included turnover frequency (TOF_{urea}) calculations in the revised manuscript (**Table S6**). The results clearly show that $Cu_{24}Ru_1$/MCHS achieves the highest TOF, indicating superior intrinsic activity per metal site. Further increasing the Ru content (e.g., $Cu_{24}Ru_2$/MCHS) led to a decline in both urea yield and TOF.

Based on the product distribution analysis of monometallic catalysts (where Ru/MCHS favors H_2 evolution and Cu/MCHS tends to form nitrite), we infer that Ru sites primarily facilitate hydrogenation steps and HER. An optimal amount of Ru promotes the necessary hydrogenation for C–N coupling, while excessive Ru diverts more *H toward HER and over-hydrogenation, thereby suppressing urea formation. Thus, the Cu:Ru = 24:1 ratio represents the optimal balance, enabling effective synergy between Cu and Ru while maximizing the utilization efficiency of the precious Ru metal.

We have added these TOF data and a more detailed discussion regarding the ratio optimization in the revised manuscript. We believe this clarification strengthens the rationale behind our catalyst design.

The relevant revisions are presented as follows:

Line 199: "We have systematically evaluated the urea synthesis performance of CuRu/MCHS catalysts with varying Ru loadings (**Fig. 3c**). The urea production rate exhibited a distinct volcano-type dependence on Ru content, with the Cu:Ru = 24:1 ratio demonstrating the highest yield. This catalyst also achieved the highest turnover frequency (TOF) among all compositions

(**Table S6**), confirming its superior intrinsic activity and optimal atomic utilization efficiency. These findings indicate that an optimal Ru content is critical for promoting the deep reduction of NO_2^- intermediates while appropriately regulating the *H supply—directing it toward C–N coupling rather than hydrogen evolution, thereby maximizing urea formation.”

Supplementary Table S6| The TOF of $Cu_{24}Ru_2$/MCHS, $Cu_{24}Ru_1$/MCHS, $Cu_{24}Ru_{0.5}$/MCHS.

Samples	Yield rate ($g\ h^{-1}\ g_{cat}^{-1}$)	TOF (Cu+Ru) ($\times10^{-2}\ s^{-1}$)
$Cu_{24}Ru_2$/MCHS	2.154	0.185
$Cu_{24}Ru_1$/MCHS	3.743	0.338
$Cu_{24}Ru_{0.5}$/MCHS	2.977	0.274

* The turnover frequency (TOF) are calculated as $TOF_{urea} = \frac{n_{urea}}{t \times n_{cat.}}$, where $n_{cat.}$ is the total loading amount of catalysts, n_{urea} is the amount of urea, and t is the reaction time.
** The average urea yield was used to calculate the TOF.

3. The urea FE remains moderate (~16.5%). While high current density is achieved, discussion on improving selectivity further would add depth. Please see doi.org/10.1002/adfm.202200882 and other relevant papers.

Response: We thank you for this insightful comment and for pointing us to the highly relevant reference. We agree that achieving higher FE remains a central challenge and a key goal for the practical implementation of urea electrosynthesis. Our current work primarily demonstrates that the nano-confinement strategy is highly effective in boosting the urea yield and stabilizing the reaction at industrial-scale current densities, which itself is a significant hurdle to overcome. The current moderate FE indeed indicates substantial competition from side reactions, primarily the HER and the diversion of nitrogen species to ammonium.

Building on this foundation and inspired by your suggestion, we have added a dedicated paragraph in the Conclusion section of the revised manuscript to discuss prospective pathways for enhancing selectivity. Our analysis, including the cited work, points to several promising directions including precise modulation of the active site microenvironment, further optimization of intermediate binding energetics, or electrode and reactor engineering. We

believe that the nano-confinement architecture we developed provides a versatile platform onto which these additional selectivity-enhancing strategies can be grafted. We have revised the manuscript to include this forward-looking discussion, framing our current achievement as a critical step that opens the door to further systematic optimization of the FE. We thank you again for this valuable suggestion.

The relevant revisions are presented as follows:

Line 452: "In summary, we have demonstrated that a nano-confinement architecture effectively overcame kinetic and diffusion limitations in the co-reduction of CO_2 and NO_3^-, achieving a 2.5-fold enhancement in urea yield compared to non-confined systems. This work establishes a nano-confinement strategy for the rational design of C–N coupling electrocatalysts. First, the synergy between CuRu bimetallic nanoclusters and the nano-confined environment enhances the adsorption of reactants and intermediates, enabling high urea production rates at industrial-scale current densities. Second, the confined pore channels and cavities facilitate the overcoming of C–N coupling energy barriers, shifting the key bonding step from the conventional COOH–NH_2 pathway to the earlier and kinetically favored OCO–NO intermediate coupling. Third, precise engineering of pore sizes optimizes the diffusion and distribution of reactants and intermediates, balancing reaction kinetics and significantly improving urea productivity and selectivity. Further efforts should prioritize mitigating side reactions and enhancing urea recovery. To enhance FE, strategies including the precise modulation of the active-site microenvironment to suppress hydrogen evolution and regulate intermediate adsorption, optimization of the metal active centers with tailored electronic structures, more advanced reactor designs that enhance local reactant concentrations, could built upon our nano-confinement platform to substantially boost selectivity[67,68]."

Newly added references:

67 Mukherjee, J. *et al.* Understanding the site-selective electrocatalytic Co-reduction mechanism for green urea synthesis using copper phthalocyanine nanotubes. *Adv. Funct. Mater.* **32**, 2200882 (2022).

68 Lai, W., *et al.* Design strategies for markedly enhancing energy efficiency in the electrocatalytic CO2 reduction reaction. *Energy Environ. Sci.* **15**, 3603-3629 (2022).

4. Table S7 compares performance with other catalysts. It would be more effective to bring a brief version into the main text for quick reader access.

Response: We thank you for this valuable suggestion. In response, we have revised **Fig. 3g** in the main text to provide a more concise and visualized comparison of catalyst performance based on the data in **Table S8**, which corresponds to the previous **Table S7**. This figure categorizes catalysts by device configuration (H-cell and flow-cell) and highlights the superior urea yield of our CuRu/MCHS catalyst under industrial-relevant current densities. Additionally, to provide a more rigorous activity comparison, we have added a new **Fig. S22** to compare the partial current density for urea formation among different catalysts, offering an intuitive and fair assessment of catalytic performance across different studies.

The relevant revisions are presented as follows:

Line 230: "This value surpasses those of all previously reported bimetallic or carbon-based catalysts under comparable conditions, exhibiting a 3.4 to 41.2-fold enhancement in flow cells (**Fig. 3g** and **Table S8**)[11,19]. In addition, the urea partial current density (j_{Urea}), a key indicator of actual production efficiency[43], reached a maximum of 22.1 mA cm^{-2} at –1.0 V (vs. RHE), and maintained 16.07 mA cm^{-2} even at a total current density of 250 mA cm^{-2}. These values significantly exceed those reported in most previous studies, which typically remain below 1–5 mA cm^{-2} (**Fig. S22**)."

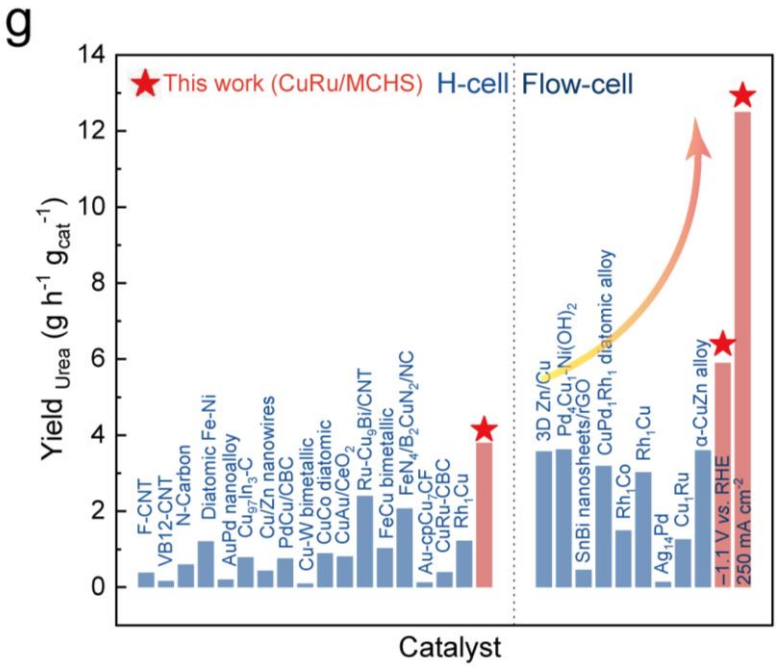

Fig. 3| Urea electrosynthesis performance of nano-confined and non-confined based electrocatalyst. g, Comparison of urea formation rate between CuRu/MCHS and other bimetallic catalysts reported in the literature. Corresponding values are tabulated in **Table S8**.

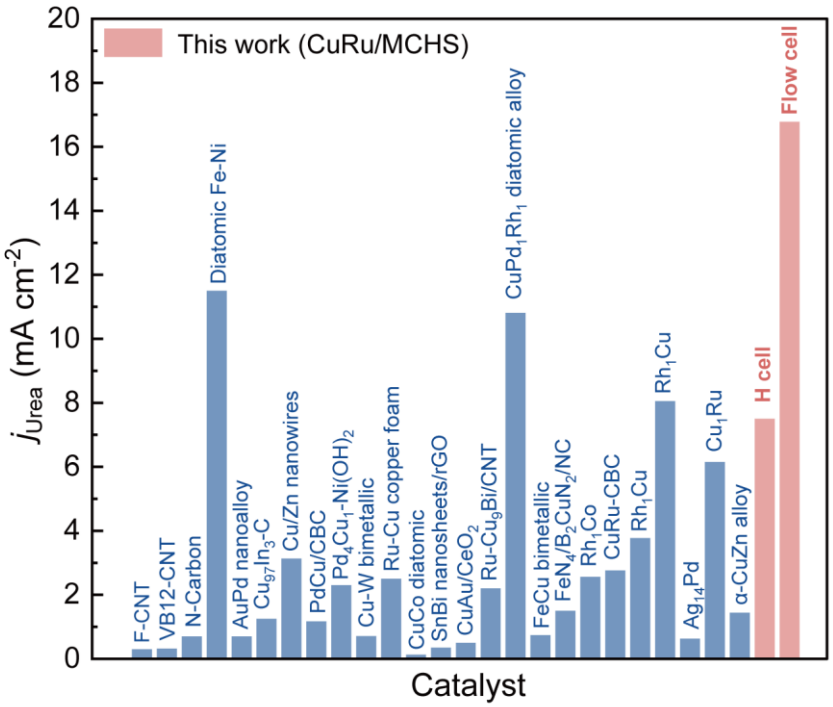

Supplementary Fig. S22| Comparison of j_{Urea} between CuRu/MCHS and other bimetallic catalysts reported in the literatures. Corresponding values are tabulated in the Table S8.

Reviewer 4

Comments: *In this manuscript, the authors developed a catalyst of CuRu bimetallic on mesoporous carbon hollow spheres (CuRu/MCHS) for urea synthesis. The authors have designed this catalyst material and conducted comprehensive experimental characterization, demonstrating the uniform dispersion of CuRu nanoparticles within the carbon layer and systematically investigating the metal valence states. However, the catalytic performance shows a considerable gap compared with most reported materials in the literature. Furthermore, several critical factors were overlooked in the DFT calculations, leading to insufficiently clear interpretation of the reaction mechanism. Therefore, based on the identified limitations in both catalytic performance and theoretical analysis, I conclude that this manuscript does not meet the scientific standards required for publication in Nature Communications. My main concerns are as follows:*

Response: We sincerely thank you for your thorough evaluation and constructive feedback on our manuscript. We appreciate your acknowledgment of the systematic catalyst design and comprehensive characterization.

Regarding the catalytic performance, we acknowledge that the FE for urea formation appears moderate compared with some reported systems. However, our work prioritizes achieving **industrially relevant urea yield rates at high current densities**, which are often accompanied by lower FE values due to intensified mass transfer and competing side reactions. We have revised **Table S8 to include a more detailed comparison with previous studies.** We have supplemented the comparison with literature data by including the current densities and applied potentials, and we further calculated the partial current density for urea (j_{Urea}) based on the reported FE_{Urea} values. A high partial current density means that more product is generated per unit electrode area and time, which directly reflects the productivity. This additional comparison highlights more clearly that **our work achieves a significantly higher j_{Urea}.** According to our analysis, the extremely high FE values reported in previous studies are typically obtained under very low current densities (j_{Urea} < 2 mA cm^{-2}), with limited consideration of catalytic activity under high or industrial-level current densities. In practical applications, electrolyzers generally operate at current densities in the range of hundreds of

milliamperes to several amperes per square centimeter, where intensified side reactions markedly reduce both FE and productivity. High current densities also introduce several challenges, including mass transport limitations, changes in local electrode pH, restrictions in electrolyte/gas supply, gas accumulation or detachment issues at the electrode surface, and increased competitive reactions (such as HER). Therefore, the high FE achieved under low current densities in laboratory-scale tests does not necessarily meet the requirements for practical production. Although research on electrochemical urea synthesis has not yet reached the pilot-scale stage, we aimed to address these practical limitations early on. Thus, our work represents an initial exploration of catalyst design and mass transport optimization under relatively high current densities.

As shown in **Fig. 3** and **Table S8**, our CuRu/MCHS catalyst delivered a urea yield rate of 12.51 g h^{-1} g_{cat}^{-1} (surpassing previous benchmarks by 3.4-fold) at 250 mA cm^{-2} in flow cell with a j_{Urea} of 16 mA cm^{-2}. These values are among the highest reported values for CO_2 and NO_3^- co-reduction systems under comparable conditions. It is noteworthy that the FE_{Urea} was further improved to 19.4 ± 4.5% in the flow cell, reaching a maximum of 22.6% with j_{Urea} of 22.1 mA cm^{-2}, which is fully comparable to most reported studies. These results collectively demonstrate that our primary goal, which was achieving ultra-high urea production rate under industrial-relevant current densities, has been successfully realized, establishing a new benchmark for scalable electrocatalytic urea synthesis. We have clarified this point in the revised manuscript and provided more detailed performance comparisons in the main text.

Regarding the DFT analysis, we agree that further clarification was needed. In the previous manuscript, we primarily focused on discussing the effect of the CuRu bimetallic system on the catalytic pathway, while incorporating FEM analysis to demonstrate the nano-confinement role of MCHS. Your suggestion regarding the inclusion of single-metal reaction pathways and the consideration of the MCHS effect on reaction energy barriers is indeed important. Therefore, we have re-evaluated and revised the entire DFT section accordingly. In the revised manuscript, to ensure the computational feasibility and rationality of the DFT analysis, **we introduced a carbon layer as the support for the nanocluster structure and re-calculated all energies again**. The energy barrier data for single-metal catalyst control was also

supplemented. Detailed descriptions of the computational models and their construction rationale are further addressed in our response to your Comment 6. The refinement of the DFT analysis has significantly improved the accuracy and completeness of the mechanistic discussion in this work.

We have carefully addressed each of your comments in the revised manuscript and believe these revisions significantly enhance the scientific rigor and clarity of our work. We thank you again for your valuable guidance.

1. The figure citation in the manuscript contains an error: "Fig. 2i-2k" should be corrected to "Fig. 1i-1k".

Response: We are very sorry for this error. The figure citation has been corrected in the revised manuscript. “Fig. 2i–2k” has been updated to “Fig. 1i–1k” to accurately reflect the intended figures. We have carefully checked the revised manuscript to ensure that no similar errors remained. We appreciated your attention to this matter.

The relevant revisions are presented as follows:

Line 100: “The EDS mapping and line-scan indicated the high dispersion of Cu and Ru on MCHS (**Fig. 1h**), forming CuRu nanoclusters (average diameters of 2.08±0.61 nm) dispersed throughout the channels and cavities (**Figs. 1i-1k** and **Fig. S4**).**”**

2. The peak positions labeled for CuRu/MCHS and Ru/MCHS in Fig. 2c are incorrect.

Response: Thank you very much for your careful reading. We have carefully checked and corrected the peak positions labeled for CuRu/MCHS and Ru/MCHS in **Fig. 2c** to ensure they accurately represent the experimental data, specifically adjusting the Ru(0) peak position labeling for CuRu/MCHS and Ru/MCHS. We sincerely thank you again for pointing this out.

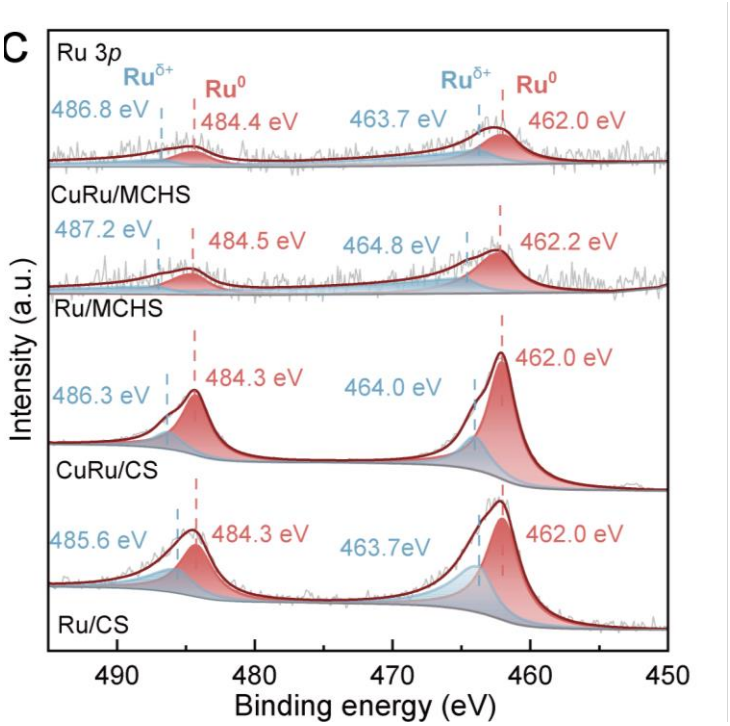

Fig. 2| Characterization of nanoconfined and non-confined based electrocatalyst. c, Ru 3p XPS spectrum.

3. The XANES analysis demonstrates that the Cu species in both CuRu/MCHS and Cu/MCHS catalysts exhibit mixed valence states between Cu(0) and Cu(I), as evidenced by the characteristic Cu-O bonding in Fig. 1f, indicating partial oxidation of Cu. However, the origin of this oxidation state (whether intrinsic to the synthesis process or resulting from post-synthetic air exposure) remains unaddressed, and the relative proportions of Cu(0) and Cu(I) species have not been quantitatively determined.

Response: We sincerely thank you for raising this important point regarding the origin and quantification of Cu oxidation states. To address this, we additionally performed XPS LMM analysis to quantify the Cu(0) and Cu(I) ratios in CuRu/MCHS and CuRu/CS. The results confirm the coexistence of both species, with Cu(0) being the predominant state.

The absence of characteristic Cu_2O diffraction peaks in XRD patterns (**Fig. S6a**) indicates that no bulk crystalline Cu_2O phase was formed during synthesis. We attribute the observed surface oxidation primarily to inevitable air exposure during sample transfer for characterization, a

phenomenon commonly reported in Cu-based electrocatalysts. This interpretation is supported by references documenting similar surface oxidation in analogous catalytic systems (*Nat Commun*. 15, 7477 (2024), *Nat. Commun.* 14, 3767, (2023), *Appl. Surf. Sci*. 255, 2730-2734, (2008)).

It should be noted that our synthesis was conducted under a 5% H_2/Ar atmosphere specifically to minimize oxidation, and all electrochemical tests were preceded by an in situ cyclic voltammetry activation protocol to reduce surface oxides. We have incorporated this quantitative analysis and corresponding discussion into the revised manuscript, providing a more comprehensive understanding of the catalyst's oxidation state.

The relevant revisions are presented as follows:

Line 119: "By quantifying the content of Cu^0 and Cu^{1+} in the Cu LMM spectra (**Fig. S6d**), the high proportion of Cu^0 was found in CuRu/MCHS (75.1%) and CuRu/CS (80.3%).**"**

Line 121: "In X-ray absorption near-edge structure (XANES), the Cu K-edge spectra showed that the pre-edge absorption energy of CuRu/MCHS and CuRu/CS were located between those of Cu foil and Cu_2O references, implying the coexistence of metallic Cu (Cu^0) and Cu(I) oxide (Cu^+) phases (**Fig. 2d**). The minor Cu^+ component likely originated from superficial oxidation during post-synthetic air exposure of the catalysts[37].**"**

Line 536: "The working electrode was activated and stabilized by cyclic voltammetry prior to testing with a 20-turn sweep under a potential window of 0 to –2 V (vs. Ag/AgCl).**"**

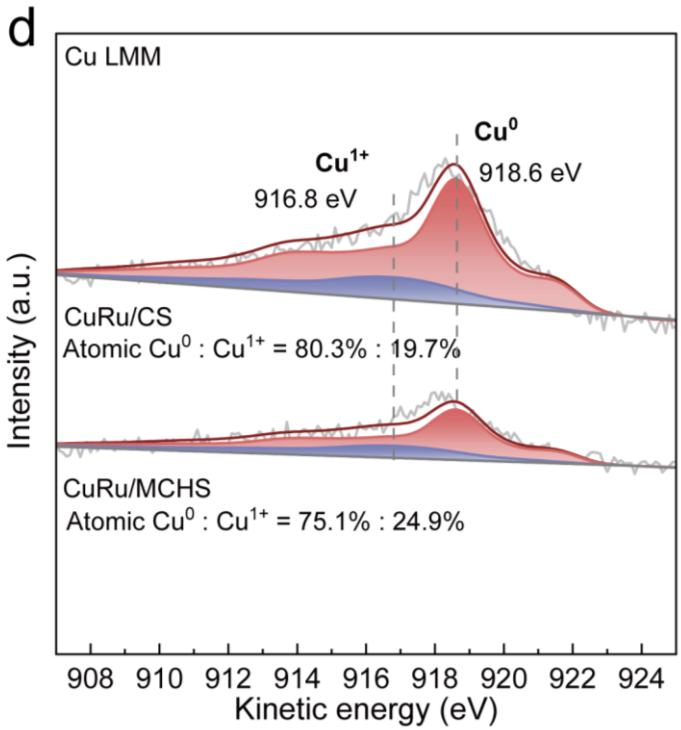

Supplementary Fig. S6| XRD and XPS characterization of samples. d, Cu LMM spectra of CuRu/MCHS and CuRu/CS.

Newly added references:

37 Wang, X. *et al.* Embedding oxophilic rare-earth single atom in platinum nanoclusters for efficient hydrogen electro-oxidation. *Nat. Commun.* **14**, 3767 (2023).

4. The reported catalyst exhibits a maximum urea Faradaic efficiency of merely 16.5%, significantly lower than the benchmark performance (>30%) achieved by most state-of-the-art catalysts in literature. Such inferior catalytic activity would severely limit its practical application for efficient urea synthesis.

Response: We thank you for raising this important point regarding the FE. We acknowledge that the maximum FE of 16.5% in H-cell is moderate when compared to some reports under lower current densities than ours. We further improved the FE to 19.4 ± 4.5% in the flow cell, achieving a maximum FE_{Urea} of 22.6% with j_{Urea} of 22.1 mA cm^{-2}. However, we respectfully propose that the practical potential of an electrocatalyst be evaluated based on a comprehensive set of metrics, particularly under industrially relevant conditions.

The primary focus and achievement of our work lie in demonstrating that the nano-confinement strategy enables an outstanding urea yield (**Fig. R3**), which is the most critical parameter for practical application as it determines the total production output by combining conversion efficiency and selectivity (i.e., FE). In addition, the catalyst exhibits exceptional stability at high current densities. To better highlight the advancement of our catalyst performance, we have enhanced the description in the main text, explicitly comparing our yield metrics with prior works under comparable high-current conditions. As highlighted in our manuscript, our CuRu/MCHS catalyst achieves a record urea yield rate of 12.51 g h^{-1} g_{cat}^{-1} at 250 mA cm^{-2} in a flow cell, surpassing previous benchmarks by 3.4-41.2 fold. The system achieves a partial current density for urea production of 16 mA cm^{-2}. This metric is increasingly recognized in the field as a crucial indicator of practical viability, complementing the FE by reflecting the actual production efficiency.

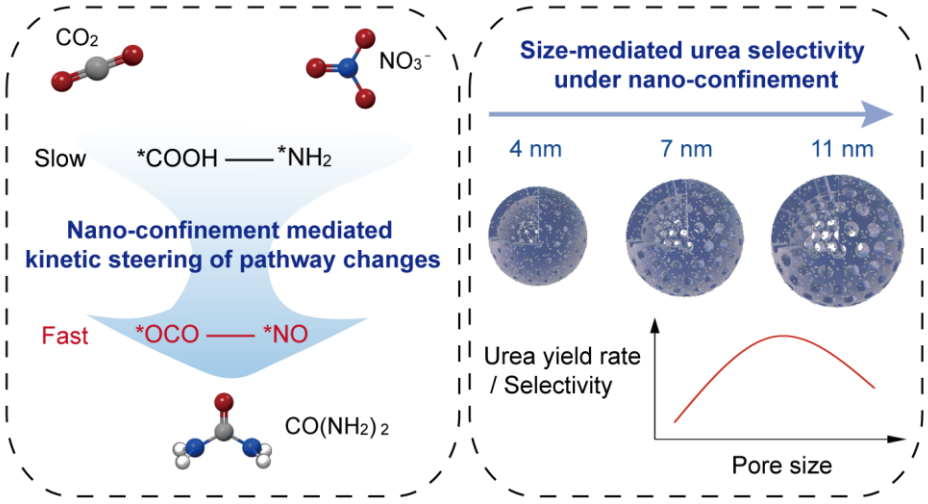

Fig. R3 Schematic illustration of the primary focus and achievement of the nano-confinement strategy in CuRu/MCHS.

It is widely observed in electrocatalysis that pushing to higher current densities for greater production rates inevitably intensifies competing reactions (like HER), leading to an FE decrease. Our work provides a viable solution to this challenge by maintaining a significant production rate and robust stability at such high currents, which is a crucial step toward industrial application. Furthermore, we have now incorporated a dedicated outlook in the Conclusion section, discussing specific strategies (e.g., precise modulation of the active-site

microenvironment and optimization of metal centers) to further enhance FE in future studies. This forward-looking discussion, combined with the key innovation of our study (i.e., the mechanistic discovery of how nano-confinement alters the C–N coupling pathway) offers a new design principle that can be utilized to develop next-generation catalysts with both high activity and high selectivity.

We have revised the manuscript to better frame our performance metrics within this context, emphasizing the significance of achieving high yield at high current density while providing a clear pathway for future FE improvement. We appreciate this constructive feedback, as addressing it has provided us with a valuable opportunity to refine our discussion on the innovation and comparative advantages of our catalyst, more sharply highlighting its progress beyond previous systems.

The relevant revisions are presented as follows:

Line 227: "Meanwhile, benefiting from the enhanced three-phase interfacial mass transfer effect, the flow cell increased the urea FE to 19.4 ± 4.5% at –1.0 V (vs. RHE) (**Fig. S21d**). Notably, at an industrial-level current density of 250 mA cm^{-2}, CuRu/MCHS achieved a record urea yield rate of 12.51 g h^{-1} g_{cat}^{-1}. This value surpasses those of all previously reported bimetallic or carbon-based catalysts under comparable conditions, exhibiting a 3.4 to 41.2-fold enhancement in flow cells (**Fig. 3g** and **Table S8**)[11,19]. In addition, the urea partial current density (j_{Urea}), a key indicator of actual production efficiency[43], reached a maximum of 22.1 mA cm^{-2} at –1.0 V (vs. RHE), and maintained 16.07 mA cm^{-2} even at a total current density of 250 mA cm^{-2}. These values significantly exceed those reported in most previous studies, which typically remain below 1–5 mA cm^{-2} (**Fig. S22**). Note that our FEs were achieved under current densities substantially higher than those employed in most prior works reporting higher FE values, and are fully comparable to those of other state-of-the-art catalysts when evaluated under similar high-current conditions[12,44-46]. The simultaneous realization of a record yield rate and high j_{Urea} at 250 mA cm^{-2} validates the unique capability of our nano-confinement strategy in overcoming the fundamental challenge of mass transport limitations, thereby maximizing urea production under industrially relevant conditions.**"**

Line 452: "In summary, we have demonstrated that a nano-confinement architecture effectively overcame kinetic and diffusion limitations in the co-reduction of CO_2 and NO_3^-, achieving a 2.5-fold enhancement in urea yield compared to non-confined systems. This work establishes a nano-confinement strategy for the rational design of C–N coupling electrocatalysts. First, the synergy between CuRu bimetallic nanoclusters and the nano-confined environment enhances the adsorption of reactants and intermediates, enabling high urea production rates at industrial-scale current densities. Second, the confined pore channels and cavities facilitate the overcoming of C–N coupling energy barriers, shifting the key bonding step from the conventional COOH–NH_2 pathway to the earlier and kinetically favored OCO–NO intermediate coupling. Third, precise engineering of pore sizes optimizes the diffusion and distribution of reactants and intermediates, balancing reaction kinetics and significantly improving urea productivity and selectivity. Further efforts should prioritize mitigating side reactions and enhancing urea recovery. To enhance FE, strategies including the precise modulation of the active-site microenvironment to suppress hydrogen evolution and regulate intermediate adsorption, optimization of the metal active centers with tailored electronic structures, more advanced reactor designs that enhance local reactant concentrations, could be built upon our nano-confinement platform to substantially boost selectivity[67,68]."

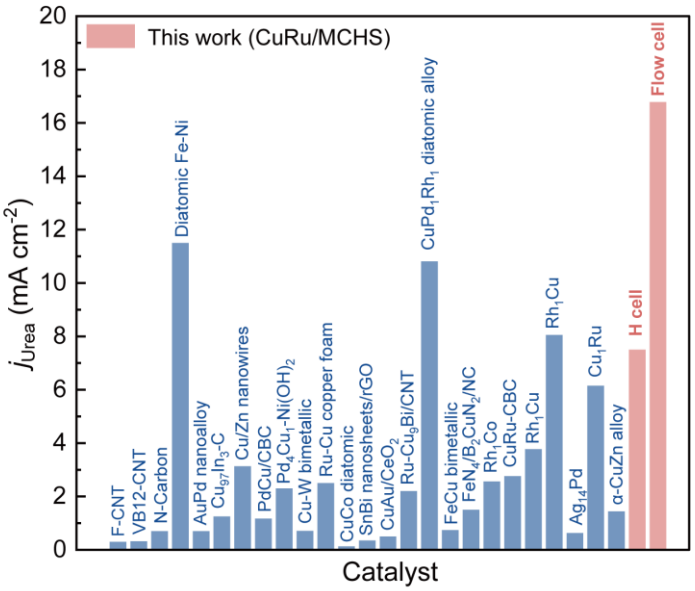

Supplementary Fig. S22| Comparison of j_{Urea} between CuRu/MCHS and other bimetallic catalysts reported in the literatures. Corresponding values are tabulated in the Table S8.

Supplementary Table S8| A comparison of urea FEs and production rate of urea between our catalysts and state-of-the-art metal and carbon based catalysts in literature.

Catalysts	Cell type	Electrolyte	Yield rate (g h^{-1} g_{cat}^{-1})	FE (Voltage) (%)	j_{Urea} (mA cm^{-2})	Ref.
F-doped CNT	H-cell	0.1 M KNO_3	0.382	18 (-0.65 V vs. RHE) ~3 (-0.85 V vs. RHE)	0.3	2
VB12-CNT	H-cell	0.1 M KNO_3	0.164	26.04 (-0.5 V vs. RHE) ~10 (-0.8 V vs. RHE)	~0.32	3
Nitrogen-doped carbon	H-cell	0.1 M KNO_3+0.1 M $KHCO_3$	0.596	62 (-0.3 V vs. RHE) ~5 (-0.7 V vs. RHE)	~ 0.7	4
Diatomic Fe-Ni	H-cell	0.05 M KNO_3+0.1 M $KHCO_3$	1.21	17.8 (-1.5 V vs. RHE) ~8 (-1.6 V vs. RHE)	~ 11.5	5
AuPd nanoalloy	H-cell	0.025 M KNO_3+0.075 $KHCO_3$	0.204	15.6 (-0.4 V vs. RHE)	~0.7	6
$Cu_{97}In_3$-C	H-cell	0.01 M KNO_3+0.1 M $KHCO_3$	0.786	5 (-1.5 V vs. RHE)	~1.25	7
Cu@Zn nanowires	H-cell	0.1 M KNO_3+0.2 M $KHCO_3$	0.437 g h^{-1} cm^{-2}	9.28 (-1.02 V vs. RHE) ~4.5 (-1.85 V vs. RHE)	3.13	8
PdCu/CBC	H-cell	0.05 M KNO_3	0.76	58.7 (-0.4 V vs. RHE) ~10 (-0.7 V vs. RHE)	~1.17	9
3D Zn/Cu hybrid catalyst	Flow cell	0.02 M KNO_3	3.57	63 (-0.6 V vs. RHE) ~35 (-0.9 V vs. RHE)	NA	10
Pd_4Cu_1-$Ni(OH)_2$	Flow cell	0.1 M KNO_3+0.1 M $KHCO_3$	3.628	64.4 (-0.5 V vs. RHE)	2.30	11

Cu-W bimetallic	H-cell	0.1 M KNO_3	0.098	70.1 (-0.2 V vs. RHE) ~5 (-0.5 V vs. RHE)	0.71	12
Ru-Cu copper foam	Single-cell	0.1 M $NaNO_3$	0.151 g h^{-1} cm^{-2}	25.4 (0.13 V vs. RHE)	~2.50	13
CuCo diatomic catalyst	H-cell	0.1 M KNO_3+0.1 M $KHCO_3$	0.89	44.04 (-0.35 V vs. RHE) ~5 (-0.75 V vs. RHE)	~0.13	14
SnBi nanosheets/ rGO	Flow cell	0.1 M KNO_3+0.1 M $KHCO_3$	0.46	78.36 (-0.4 V vs. RHE) ~7 (-0.55 V vs. RHE)	~0.35	15
$CuAu/CeO_2$	H-cell	0.1 M KNO_3	0.813	45.2 (-0.74 V vs. RHE) ~21 (-1.0 V vs. RHE)	~0.5	16
Ru-Cu_9Bi/CNT	H-cell	0.1 M KNO_3+0.1 M $KHCO_3$	2.4	74.8 (-0.4 V vs. RHE) ~8 (-0.7 V vs. RHE)	~2.2	17
$CuPd_1Rh_1$ diatomic alloy	Flow cell	0.1 M KNO_3+0.1 M $KHCO_3$	3.19	72.1 (-0.5 V vs. RHE) ~20 (-0.7 V vs. RHE)	~10.81	18
FeCu bimetallic clusters	H-cell	0.1 M KNO_3	1.024	39.8 (-0.5 V vs. RHE) ~17 (-0.7 V vs. RHE)	0.74	19
FeN_4/B_2CuN_2@NC	H-cell	0.1 M KNO_3+0.1 M $KHCO_3$	2.073	71.9 (-0.4 V vs. RHE) ~5 (-0.7 V vs. RHE)	1.5	20
Au@cpCu_7 CF	H-cell	8 mM KNO_3+0.2 M $KHCO_3$	0.126	55.53 (Pulse potential: -0.2/-0.6 V vs. RHE)	NA	21
Rh_1Co	Flow cell	0.1 M KNO_3+0.1 M $KHCO_3$	1.495	51.1 (-0.6 V vs. RHE) ~15 (-0.8 V vs. RHE)	~2.56	22
CuRu-CBC	H-cell	0.1 M KNO_3	0.394	68.94 (-0.55 V vs. RHE)	~2.76	23

				~18 (-0.65 V vs. RHE)		
Rh_1Cu	H-cell	0.1 M KNO_3+0.1 M $KHCO_3$	1.219	62.96 (-0.6 V vs. RHE)	~3.77	24
	Flow cell	0.1 M KNO_3+0.1 M $KHCO_3$	3.024	67.1 (-0.6 V vs. RHE)	~8.05	
$Ag_{14}Pd$	Flow cell	200 ppm NO_3–N+1 M KOH	0.143	15.8 (-0.276 V vs. RHE) ~3 (-0.576 V vs. RHE)	~0.63	25
Cu_1Ru	Flow cell	0.1 M KNO_3+0.1 M $KHCO_3$	1.263	51.27 (-0.6 V vs. RHE) ~30 (-0.8 V vs. RHE)	~6.15	26
α-CuZn alloy	Flow cell	0.02 M KNO_3+0.2 M $KHCO_3$	3.6	28.7% (-0.42 V vs. RHE) ~10% (-0.62 V vs. RHE)	~1.44	27
CuRu/MCHS-7	H-cell	0.1 M KNO_3	3.6 (–1.1 V vs. RHE)	16.5±1.2 (-1.1 V vs. RHE)	7.5	This work
	Flow cell		5.9 (–1.1 V vs. RHE)	19.4 ± 4.5 (-1.0 V vs. RHE)	16.78	
	Flow cell (250 mA cm^{-2})		12.5	6.4	16.07	

* "~" observed or calculated from research data.

Newly added references:

43 Dutta, N. *et al.* A guideline to determine faradaic efficiency in electrochemical CO_2 reduction. *ACS Energy Lett.* **9**, 323-328 (2024).

44 Meng, N. *et al.* Oxide-Derived Core–Shell Cu@Zn Nanowires for Urea Electrosynthesis from Carbon Dioxide and Nitrate in Water. *ACS Nano* **16**, 9095-9104 (2022).

45 Liu, Y. *et al.* C-Bound or O-Bound Surface: Which one boosts electrocatalytic urea synthesis? *Angew. Chem. Int. Ed.* **62**, e202300387 (2023).

46 Zhai, S. *et al.* Brass phase determining selectivity in urea electrosynthesis from CO_2 and nitrate. *ACS Catal.* **15**, 3276-3283 (2025).
67 Mukherjee, J. *et al.* Understanding the site-selective electrocatalytic co-reduction mechanism for green urea synthesis using copper phthalocyanine nanotubes. *Adv. Funct. Mater.* **32**, 2200882 (2022).
68 Lai, W., *et al.* Design strategies for markedly enhancing energy efficiency in the electrocatalytic CO_2 reduction reaction. *Energy Environ. Sci.* **15**, 3603-3629 (2022).

5. The Faradaic efficiency for urea production was not evaluated in the flow cell system, which represents a critical electrochemical metric for evaluating catalytic performance.

Response: We appreciated your insightful suggestion regarding the FE in the flow cell as an important metric for evaluating catalytic activity. Based on your suggestion, we have now supplemented the FE data in the flow cell. The results have now been included in the main text to provide a complete assessment of the catalytic performance.

The relevant revisions are presented as follows:

Line 227: "Meanwhile, benefiting from the enhanced three-phase interfacial mass transfer effect, the flow cell increased the urea FE to 19.4 ± 4.5% at –1.0 V (vs. RHE) (**Fig. S21d**)**."**

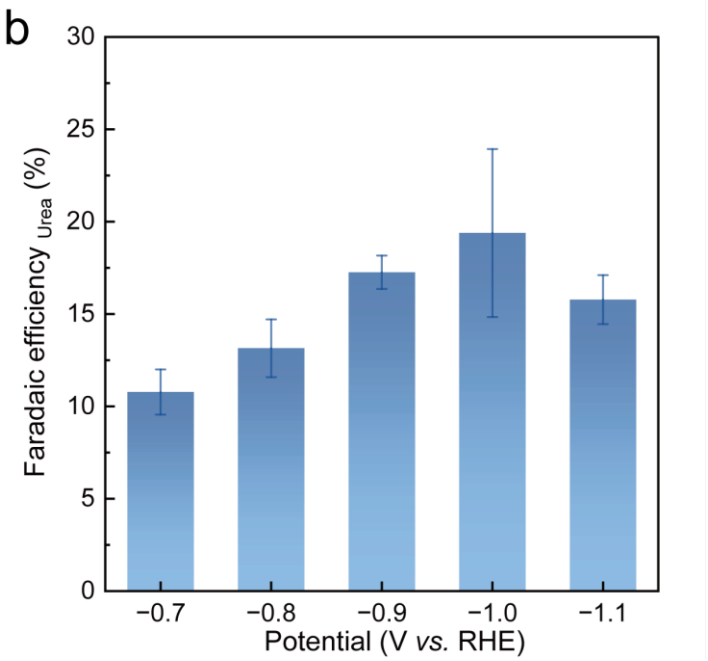

Supplementary Fig. S21| Performance of electrocatalytic CO_2 and NO_3^- co-reduction by CuRu/MCHS in flow cell. d, FE of urea performance at various potential in flow cell.

6. The presented DFT calculations are notably incomplete as the authors neither consider the essential control cases of urea synthesis on pure Cu and pure Ru for mechanistic comparison, nor do they consider the potential role of the MCHS support structure.

Response: We thank you for this critical insight regarding the scope of our DFT analysis. We agree that considering support effects and including control comparisons are essential for a comprehensive mechanistic understanding. In the revised manuscript, we have substantially expanded our computational study to address these points.

First, following established approaches in the literature for carbon-supported metal catalysts (e.g., *Chem* 8, 3, 749–768 (2022); *Nat. Commun.* 14, 5108 (2023); *Nat. Commun.* 14, 3767 (2023)), we adopted a carbon layer as the support for the metal catalytic model. First, we have re-calculated all the Gibbs free energies of each intermediate along the *OCONO and *$COOHNH_2$ pathways respectively on the CuRu model. By comparing the energy barriers of the two pathways, we once again confirmed the C–N bond formation barriers and the differences between the two reaction routes. The introduction of the carbon layer did not significantly affect the previously calculated energy barrier trends, but it further improved the accuracy of the energy barrier analysis for each step.

Second, we incorporated a pure Cu nanocluster model supported on carbon to directly compare its energy with the bimetallic CuRu system. By comparing the energy barriers of all steps and of individual key steps, the roles of Cu and Ru in urea synthesis along the *OCONO pathway were elucidated. Cu primarily facilitates CO_2 adsorption and hydrogenation, providing favorable sites for CO_2 activation, while its activity is modulated by the presence of Ru to favor urea formation over HCOOH. Ru plays a crucial role in reducing hydrogenation energy barriers during the PCET process and promotes the formation of key intermediates (*$COOHNH_2$ → *$CONH_2$) after the initial C–N bond formation, enhancing the overall urea synthesis along the *OCONO pathway. These newly added calculations greatly strengthened the theoretical basis for further mechanistic interpretation.

The revised computational section, along with the newly provided complete energetic data

(including zero-point energy and entropy corrections) in the Supplementary Information, now provides a more rigorous and multi-faceted theoretical foundation for our proposed mechanism. We are grateful for your guidance, which has significantly strengthened this part of our work.

The relevant revisions are presented as follows:

Supplementary information txt: "To better consider the potential role of the MCHS support structure, we included the carbon support in the computational model.**"**

Line 281: "Based on the characterizations from XPS and EXAFS analysis, a structural model with a carbon layer as the support and Ru clusters loaded on Cu clusters was constructed to simulate the CuRu structures in the CuRu/MCHS and CuRu/CS systems. Adsorption energy analyses revealed that CO_2 exhibited stronger bonding affinity with Cu (–1.58 eV) than Ru (–1.40 eV), whereas NO_3^- preferentially interacted with Ru (–1.65 eV) than Cu (–1.12 eV) (**Fig. S24a**). In the *OCONO path, the coupling between *OCO and *NO to *OCONO (i.e., the first C–N coupling step) required to overcome an energy barrier of 0.79 eV. In contrast, the *$COOHNH_2$ path exhibited a smaller energy barrier of 0.64 eV during the first C–N coupling step (*$COOH+*NH_2 \rightarrow *COOHNH_2$), yet with a much longer reaction path from *OCO and *NO (**Table S10** and **Table S11**). The subsequent proton-coupled electron transfer (PCET) process was mainly limited by the hydrogenation of *CO_2. After C–N bond formation, the energy barrier for the initial *CO_2 hydrogenation was reduced from 0.67 eV ($*OCO+*NH_2 \rightarrow *COOH+*NH_2$) to 0.33 eV ($*OCONH_2 \rightarrow *COOHNH_2$), suggesting that urea was facilely produced after the first C–N coupling.

By comparing the reaction pathways on the pure Cu cluster model, the critical role of Ru in reducing the hydrogenation energy barriers during the PCET process was verified (**Table S12**). The incorporation of Ru clusters further facilitated the formation of *OCONHO and *OCONH intermediates following the initial C–N bond formation (**Fig. S24b-d**). On the pure Cu surface, the energy barrier for the $*COOHNH_2 \rightarrow *CONH_2$ step was 0.50 eV, substantially lower than that on the CuRu surface (1.16 eV). However, the energy barrier for the first carbon-side hydrogenation step ($*OCONH_2 \rightarrow *COOHNH_2$) increased to 0.61 eV on Cu (**Fig. S25**). In addition, a lower energy barrier was observed for CO_2 reduction to *COOH on the pure Cu

surface (–0.27 eV vs. 0.03 eV on CuRu), rationalizing the preferential formation of HCOOH on Cu/MCHS. These results indicate that the presence of Ru modulates the CO_2 hydrogenation behavior on Cu, steering the pathway toward urea production instead of HCOOH.”

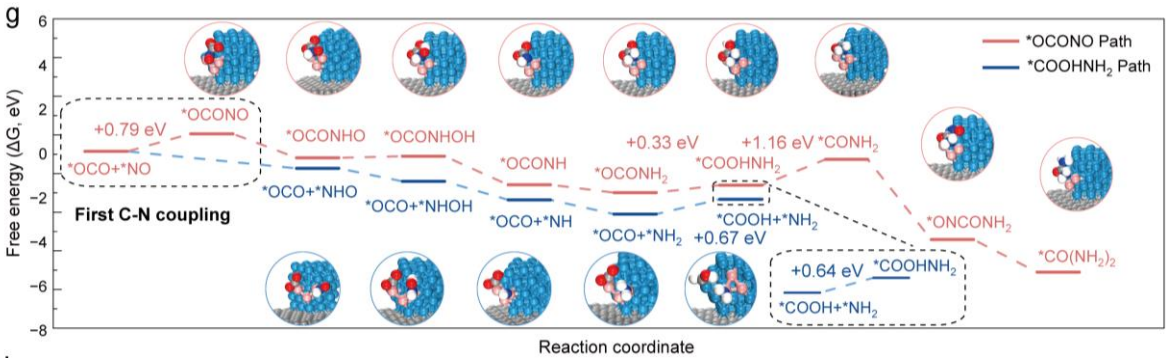

Fig. 4| Mechanistic study of CuRu/MCHS and CuRu/CS. g, Reaction diagrams evaluated by periodic DFT of urea production on CuRu surface and corresponding atomic configurations. The gray, blue, red, white, pink and turquoise balls represent C, N, O, H, Cu and Ru atoms, respectively.

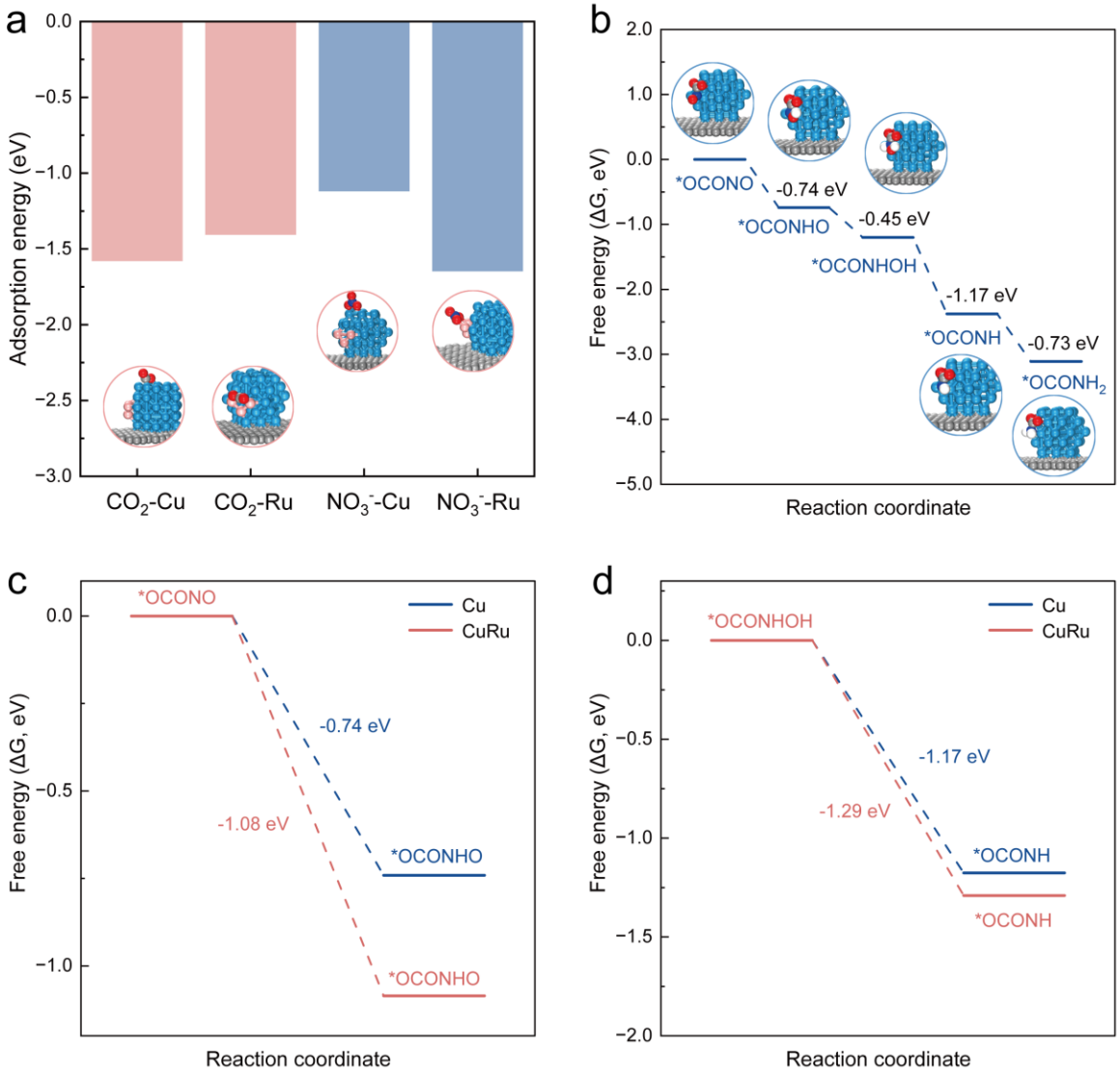

Supplementary Fig. S24| DFT calculations of urea production on CuRu and Cu surface. **a**, Comparison of CO_2 and NO_3^- adsorption energies on Cu site and Ru site of the CuRu model. **b**, Energy profiles of each elementary step in C–N coupling toward urea synthesis on the Cu model and corresponding atomic configurations. The gray, blue, red, white, pink and turquoise balls represent C, N, O, H, Cu and Ru atoms, respectively. **c**, Energy profiles of *OCONO to *OCONHO step on the CuRu and Cu model.**d**, Energy profiles of *OCONHOH to *OCONH step on the CuRu and Cu model.

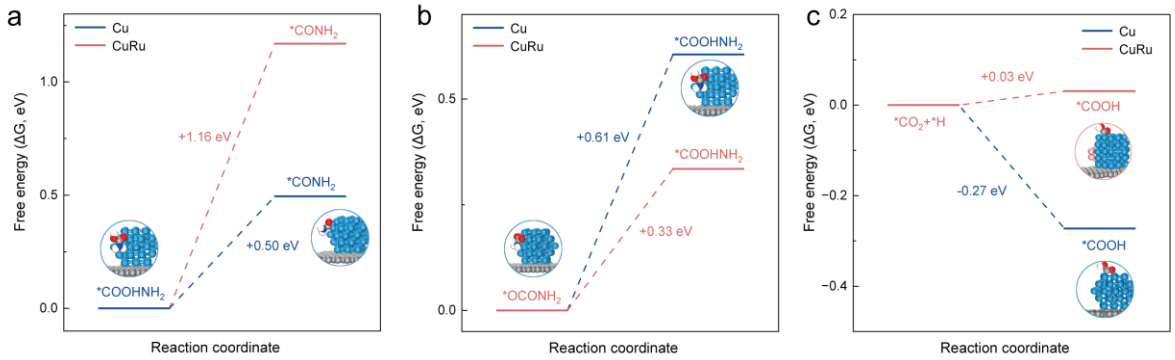

Supplementary Fig. S25| DFT calculations of CO_2RR and C–N coupling on CuRu and Cu surface. a, Energy profiles of *$COOHNH_2$ to *$CONH_2$ step on the CuRu and Cu model. **b**, Energy profiles of *$OCONH_2$ to *$COOHNH_2$ step on the CuRu and Cu model. **c**, Energy profiles of *CO_2 to *COOH step on the CuRu and Cu model. The gray, blue, red, white, pink and turquoise balls represent C, N, O, H, Cu and Ru atoms, respectively.

Supplementary Table S10| The calculated ΔE, ΔE_{ZPE} and $T\Delta S$ of various species along the reaction pathways for urea synthesis on the CuRu model .

Species	ΔE (eV)	ΔE_{ZPE} (eV)	$T\Delta S$ (eV)
HNO_3	-28.59	0.71	0.35
*CO_2	-1111.39	0.28	0.35
*COOH	-1115.20	0.60	0.38
*CO_2NO	-1126.15	0.53	0.45
*CO_2NHO	-1131.06	0.88	0.46
*CO_2NHOH	-1134.75	1.19	0.51
*CO_2NH	-1125.32	0.76	0.34
*CO_2NH_2	-1129.45	1.11	0.41
*$COOHNH_2$	-1132.78	1.39	0.51
*$CONH_2$	-1120.86	0.94	0.36
*$ONCONH_2$	-1135.95	1.23	0.41
*$CO(NH_2)$	-1137.96	1.77	0.44
*CO_2+*NO	-1126.71	0.50	0.65
*CO_2+*NHO	-1131.21	0.79	0.70
*CO_2+*NHOH	-1135.58	1.09	0.71
*CO_2+*NH	-1125.76	0.66	0.49
CO_2+NH_2	-1130.19	0.98	0.52
COOH+NH_2	-1133.12	1.27	0.68

Supplementary Table S11| The calculated free energy barriers of *COOH-NH_2 and *OCO-NO pathways for urea synthesis on the CuRu model .

Reaction coordinates	ΔG (eV)
$*CO_2+*NO \rightarrow *CO_2NO$	+0.79
$*CO_2NH_2 \rightarrow *CO_2NO$	+0.33
$*CO_2+*NH_2 \rightarrow *COOH+*NH_2$	+0.67
$*COOH+*NH_2 \rightarrow *COOHNH_2$	+0.64

Supplementary Table S13| The calculated Δ*E*, ΔE_{ZPE} and TΔ*S* of various species along the reaction pathways for urea synthesis on the Cu model.

Species	Δ*E* (eV)	ΔE_{ZPE} (eV)	*T*Δ*S* (eV)
$*CO_2$	-1088.34	0.28	0.35
*COOH	-1091.85	0.60	0.38
$*CO_2NO$	-1101.90	0.50	0.49
$*CO_2NHO$	-1106.45	0.84	0.51
$*CO_2NHOH$	-1110.58	1.16	0.66
$*CO_2NH$	-1101.16	0.76	0.40
$*CO_2NH_2$	-1105.58	1.08	0.53
$*COOHNH_2$	-1108.72	1.38	0.57
$*CONH_2$	-1097.49	0.95	0.42